
# The Hundred Thousand Proper Motions Project

prepared by: F. Mignard
affiliation : OCA
reference: GAIA-C3-TN-OCA-FM-040-01
issue: 01
revision: 0
date: 2009-10-21
status: Issued

# Abstract

This note sets forth the main technical aspects of the HTPM project, to release accurate proper motions of the Hipparcos stars few months after Gaia launch, from the combination of early Gaia astrometry with Hipparcos positions acquired 21 years before. The interest of the project in term of science and as a communication tool is recalled in the general presentation. Accurate expressions to obtain the proper motions from two positions are derived and shown to meet the accuracy requirements, even for the most difficult nearby and fast-moving stars. Results based on a realistic simulation built upon the Hipparcos Catalogue are presented and discussed. One finds that the proper motion in right-ascension can be ascertained with an accuracy (RMS of the true error) of 65 $\mu$as/yr, while this is as low as 48 $\mu$as/yr in declination. A simple error propagation model allows also to evaluate these uncertainties from only known quantities during the real exploitation. Provided the radial velocity of the 2000 nearest stars is known to within 1 to 2 km/s, the modelling error can be reduced below 10 $\mu$as/yr for these stars. It is shown that the issue is not critical for stars with parallaxes below 20 mas and that the required radial velocities are very likely available in existing databases.

# Contents

# 1 Introduction

All the Hipparcos stars to be observed by Gaia will be extremely bright, with rather constant astrometric precision of the order of 35 $\mu$as for the along scan accuracy of a single observation (9 CCDs of a FOV transit). Even though the across scan accuracy is lower by a factor around five JDB-053, this means that a single observation with a moderately accurate attitude could translate quickly into an astrometric apparent direction with an accuracy as good as one mas. Therefore after few months of observations it will be possible to have a second epoch position of most of the Hipparcos stars with an accuracy not much different from the catalogue itself when it was published, and in any case much better than the propagated position using the 1991.25 Hipparcos proper motions. Combining these two $\sim$ 1 mas accurate positions will allow us to derive a new proper motion at either epoch with an accuracy of the order of 1 mas/21 years $\approx$ 50 $\mu$as/yr. However this can only be achieved if one can determine the barycentric position of the Hipparcos stars, instead of the instantaneous apparent direction, from the few Gaia observations obtained during the first few months. The positions provided very directly by Gaia over a very short period differ from the barycentric positions essentially by the parallactic effect, since they are already corrected for the aberration. One can then take the Hipparcos parallaxes to derive barycentric positions with an accuracy of the order or smaller than the Hipparcos parallax accuracy, typically 1 mas.

This is the goal of the HTPM (**H**undred **T**housands **P**roper **M**otions) project submitted to the GST in May 2009. The GST approved the principle of this quick and very specific release, which must be turned into a DPAC proposal in CU3. This is scientifically valuable provided the release takes place early in the mission, before Gaia could improve these results with two years of data, that is to say not before 2.5 years after launch. It will rejuvenate immediately the Hipparcos Catalogue, since with this update the aging will be much slower. During the intervening years before the first release of a Gaia-only solutions, new investigations could be conducted on the galactic rotation using proper motions 20 times better than Hipparcos'. Also, astrometric reduction using Hipparcos stars for reference with their propagated positions in 1990 or 2000, could be done anew with much more accurate positions. Publishing such a result within one year after the launch will be a vivid proof that Gaia is working and could be easily publicised, given the prestige of Hipparcos in the astronomical community. This would be a beautiful and symbolic bridge between the two generations of ESA astrometry missions and a true showcase to display European leadership in this field. Finally given the capabilities and current schedules of other astrometric missions like NanoJasmine in Japan or J-MAPS in the US, this is also presented as a major objective of these smaller missions to combine their astrometric solution in 2012 or 2013 with Hipparcos, in order to get the best proper motions ever produced. So if the Gaia community can do it quickly with the early observations collected by the satellite, this must be done. This is an appealing goal demanding little extra effort atop of the normal data processing.

It is important to notice that producing these proper motions with the early Gaia positions, should not be mistaken for a Gaia data release: these positions owe very little, if anything,

to Gaia global astrometric solution, and the Gaia accuracy is in no way reflected into these positions. The main source of *noise* comes from the Hipparcos parallax uncertainty, used to refer Gaia apparent positions with a $\sim 40\mu$as accuracy along the scan direction, to barycentric positions with something between 0.5 to 1 mas accuracy. No Gaia derived parallaxes will be used in this process. In fact the full Gaia solution, for many more stars, will supersede the HTPM solution two years later, although comparing proper motions derived over a 5- and 20-year periods will be very valuable to detect unseen companions.

The GST presentation outlined the overall principles of the combination of Gaia positions with Hipparcos' and showed that it could be realised from only six months of data, when every star have been observed at least one time and many at least at two different epochs. Four month would be too short a period for this purpose. This note goes deeper into the technicalities of the project by discussing the determination of proper motions from two statistically independent positions, accurate to the milliarcsec level and separated by 21 years. This fortunate circumstance shows up for the first time in the history of astronomy and much care must be exercised in the modelling to avoid losing accuracy by relying on too approximate algorithms, not appropriate for nearby stars.

The document is organised into two largely independent parts. In the first part one shows the need for a precise definition of the proper motion compatible with high astrometric accuracy at end epochs, leading to the derivation of practical algorithms to compute the proper motion components from two well separated positions, in particular for nearby and fast moving stars. In the second part a full simulation is developed to establish the performances expected from the combination of the Hipparcos catalogue and the Gaia positions measured during the first few months of the mission, using Hipparcos parallaxes to derive the barycentric positions. The results are analysed in detail, in particular to test the validity of the algorithms obtained in the first part when used with problem stars.

# 2 Notations

TABLE 1: Various notations used throughout this document

| Symbol | Meaning | Units |
|---|---|---|
| $\alpha_0, \delta_0$ | spherical coordinates of a star at epoch $t_0$ | radians, degrees |
| $\alpha, \delta$ | spherical coordinates of a star at time $t$ | radians, degrees |
| $\mathbf{p}$ | unit vector in natural frame in the direction of increasing $\alpha$ | - |
| $\mathbf{q}$ | unit vector in natural frame in the direction of increasing $\delta$ | - |
| $r$ | distance to the star | km, pc |
| $\varpi$ | stellar parallax | mas, $\mu$as |
| $\mathbf{V}$ | velocity vector of the star | km/s |
| $V_r$ | radial velocity of the star | km/s |
| $\mathbf{W}$ | velocity vector in angular unit $(\mathbf{V}/r)$ | mas/yr, $\mu$as/yr |
| $W$ | $\lvert\mathbf{W}\rvert$ | mas/yr, $\mu$as/yr |
| $W_r$ | radial velocity of the star in angular unit $(V_r/r)$ | mas/yr, $\mu$as/yr |
| $\mathbf{W}_\perp$ | proper motion vector or on-the sky annual motion | mas/yr, $\mu$as/yr |
| $\mathbf{u}(t)$ | unit vector in the direction of a star at time $t$ | - |
| $\mathbf{u}_0$ | unit vector in the direction of a star at first epoch | - |
| $\mu_r$ | same as $W_r$: proper motion in radial direction | mas/yr, $\mu$as/yr |
| $\mu_\alpha$ | proper motion component at $t_0$ in $\alpha$ $(\frac{d\alpha}{dt}\cos\delta)_{t=t_0}$ | mas/yr, $\mu$as/yr |
| $\mu_\delta$ | proper motion component at $t_0$ in $\delta$ $(\frac{d\delta}{dt})_{t=t_0}$ | mas/yr, $\mu$as/yr |
| $\boldsymbol{\mu}$ | same as $\mathbf{W}_\perp$ | mas/yr, $\mu$as/yr |
| $\mu$ | $(\mu_\alpha^2 + \mu_\delta^2)^{1/2}$ | mas/yr, $\mu$as/yr |
| $\Delta\alpha^\star$ | $(\alpha - \alpha_0)\cos\delta_0 = \Delta\alpha\cos\delta_0$ | mas/yr, $\mu$as/yr |
| $\Delta\delta$ | $\delta - \delta_0$ | mas/yr, $\mu$as/yr |
| $a$ | same as $\Delta\alpha\cos\delta_0$ | mas/yr, $\mu$as/yr |
| $d$ | same as $\Delta\delta$ | mas/yr, $\mu$as/yr |
| $\bar{a}$ | $\Delta\alpha\cos\delta$ ($\delta$ instead of $\delta_0$) | mas/yr, $\mu$as/yr |
| $x, y$ | tangent plane coordinates (any projection) | |
| $\Gamma^k_{ij}$ | Christoffel symbol of second kind | - |
| $R_\mathrm{G}$ | Distance to galactic centre | kpc |
| $M_\mathrm{G}$ | Mass of the Galaxy | solar mass |

# Part I

# The Mathematical Framework

## 3 Kinematical model

### 3.1 General principle

Relating the sky directions of a star at two epochs $t_0$ and $t_1$ is achieved through a propagation model (also called epoch transformation) that describes the star path between its initial position at $t_0$ to its final position at $t_1$. For single stars, there has been so far no observation showing departure from the rectilinear motion in space shown in Fig. 1. The initial direction and the velocity vector $\mathbf{V}$ define the plane in which the motion takes place. The fact that the motion lies in a plane has an interesting consequence: the intersection of the plane going through the origin $O$ with the unit sphere centred at $O$ is a great circle, meaning that the projected motion takes place on a great circle of the sphere, a fact not obvious otherwise.

This simple kinematical model neglects the possible curvature of the motion in space due to the acceleration caused by the whole Galaxy or the gravitational pull by neighbouring stars. One can easily assess its validity with orders of magnitude. From the galactic rotation motion, one has a tidal acceleration (differential acceleration of the star relative to the Sun, since the solar system is also affected by the galactic potential) roughly equal to

$$\frac{GM_G}{R_G^2}\frac{r}{R_G}$$

where $M_G$ is the mass of the galactic matter inside the solar system, $R_G$ the distance to the galactic centre and $r$ the distance to the star. This acceleration is directly proportional to the star distance, meaning its contribution in angular unit is constant, equal to $GM_G/R_G^3 \sim 3 \times 10^{-4}\mu$as yr$^{-2}$. Now the average separation between two stars in the solar vicinity is about 2.5 pc, giving an angular gravitational acceleration by nearby stars of $2GM_\odot/r^3 \sim 10^{-4}\mu$as yr$^{-2}$. Therefore even after 20 years, the interval between Hipparcos and Gaia, the contribution of these accelerations to the space proper motion is negligibly small, less than 0.01 $\mu$as/yr.

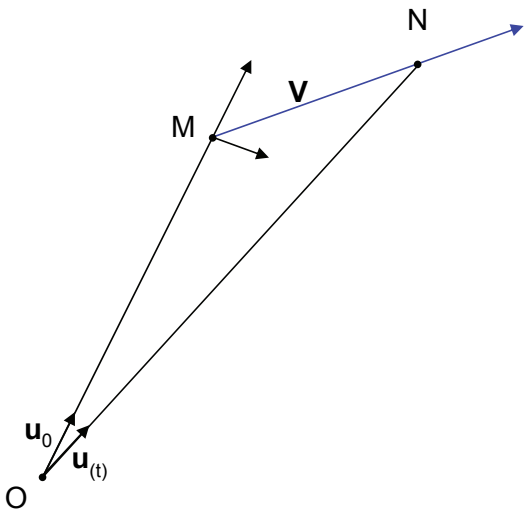


FIGURE 1: Kinematic model for the motion of a single star. This is a uniform rectilinear motion in space with velocity vector $\mathbf{V}$.

**Remark**: It is important to stress that the possibility to ignore the acceleration applies only to the 3D motion, and not to the projected angular motion, for which terms in $t^2$ are not negligible and result from the projection on the celestial sphere and not from a true accelerated motion in space. Expressing the space velocity or acceleration in angular units is not the same as converting the velocity into the angular proper motion on a great circle. The choice of the unit is just a convenient rescaling using the distance at the first epoch as unit length, without changing the nature of the motion in the euclidian space. On the other hand the projection ends up with a different motion of a fictitious object (the projection of the star) moving on a curved manifold with only two dimensions. No wonder that the kinematics might be very different.

## 3.2 The propagation equation

Based on this rectilinear motion we have the very simple propagation model,

$$\mathbf{ON}(t) = \mathbf{OM} + \mathbf{V}\,t \tag{1}$$

relating the initial star position vector at the initial epoch (here $t_0 = 0$) to the position at any time $t$. Putting

$$|\mathbf{OM}| = r \tag{2}$$

for the distance at the first epoch and using respectively $\mathbf{u}_0$ and $\mathbf{u}$ for the unit vectors in the direction of the star at $t_0 = 0$ and $t$, one has

$$\frac{\mathbf{ON}}{r} = \mathbf{u}_0 + \frac{\mathbf{V}}{r}\,t \tag{3}$$

and then with $\mathbf{W} = \mathbf{V}/r$, to express the velocity in angular unit,

$$\frac{\mathbf{ON}}{r} = \mathbf{u}_0 + \mathbf{W}\,t \tag{4}$$

and finally with $W = |\mathbf{W}|$,

$$\begin{aligned} \mathbf{u}(t) &= \frac{\mathbf{u}_0 + \mathbf{W}\,t}{|\mathbf{u}_0 + \mathbf{W}\,t|} \\ &= (\mathbf{u}_0 + \mathbf{W}\,t)\left(1 + 2\mathbf{u}_0 \cdot \mathbf{W}\,t + W^2\,t^2\right)^{-1/2} \end{aligned} \tag{5}$$

Eq. (5) is the exact form of the propagation model giving the unit direction vector at time $t$ without approximation, beyond the fact that the 3-D motion is uniform on a straight line. One can see that it depends on the three components of the velocity scaled by the distance, that is to say on the three components of the angular proper motion, including that in the radial direction.

## 3.3 Approximate expansions of the model

The small term in (5) is $Wt$, of the order of the angular displacement over the interval $t - t_0$. By expanding to third order of the small parameter, one gets

$$\begin{aligned} \mathbf{u}(t) = \mathbf{u}_0 &+ \Big[\mathbf{W} - (\mathbf{u}_0 \cdot \mathbf{W})\,\mathbf{u}_0\Big]\,t \\ &+ \Big[\big(3(\mathbf{u}_0 \cdot \mathbf{W})^2 - W^2\big)\mathbf{u}_0 - 2(\mathbf{u}_0 \cdot \mathbf{W})\,\mathbf{W}\Big]\,\frac{t^2}{2} \\ &+ \Big[\big(3(\mathbf{u}_0 \cdot \mathbf{W})\,W^2 - 5(\mathbf{u}_0 \cdot \mathbf{W})^3\big)\mathbf{u}_0 + \big(3(\mathbf{u}_0 \cdot \mathbf{W})^2 - W^2\big)\,\mathbf{W}\Big]\,\frac{t^3}{2} \end{aligned} \tag{6}$$

It is convenient to express $\mathbf{W}$ with its radial and sky components as,

$$\mathbf{W} = \mathbf{W}_\perp + W_r\,\mathbf{u}_0 \tag{7}$$

where $W_r = v_r/r$ is the radial proper motion. Then,

$$\begin{aligned} \mathbf{u}(t) = \mathbf{u}_0 &+ \mathbf{W}_\perp\,t \\ &+ \Big[\big(3W_r^2 - W^2\big)\,\mathbf{u}_0 - 2W_r\,\mathbf{W}\Big]\,\frac{t^2}{2} \\ &+ \Big[\big(3W_r\,W^2 - 5W_r^3\big)\,\mathbf{u}_0 + \big(3W_r^2 - W^2\big)\,\mathbf{W}\Big]\,\frac{t^3}{2} \end{aligned} \tag{8}$$

which can be further simplified by expressing each order with a radial and along-sky components as,

$$\begin{aligned}\mathbf{u}(t) = \mathbf{u}_0 + \mathbf{W}_\perp\, t \\ - \left[W_\perp^2 \mathbf{u}_0 + 2W_r\, \mathbf{W}_\perp\right] \frac{t^2}{2} \\ + \left[2\, W_r\, W_\perp^2 \mathbf{u}_0 + \left(2W_r^2 - W_\perp^2\right) \mathbf{W}_\perp\right] \frac{t^3}{2}\end{aligned} \tag{9}$$

The term $W_r\ \mathbf{W}_\perp$ in $t^2$ is the so-called perspective effect with its two components $\mu_\alpha\, v_r/r, \mu_\delta\, v_r/r$.

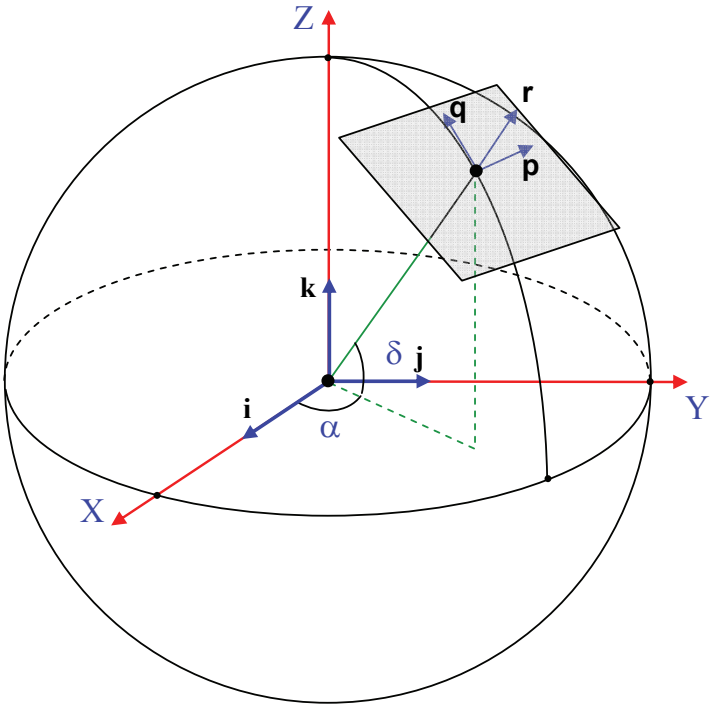


FIGURE 2: Local triad in the tangent plane associated to a unit direction vector.

Eq. 9 can be projected on the local tangent frame $[\mathbf{p}, \mathbf{q}]$ (Fig. 2) to relate the components of the displacement between two epochs to that of the proper motion components at the first epoch.

This leads to,

$$(\mathbf{u}(t)-\mathbf{u}_0)\cdot\mathbf{p} = \mu_\alpha\, t - \mu_r\,\mu_\alpha\, t^2 + (\mu_r^2 - \mu^2/2)\,\mu_\alpha\, t^3 + \mathcal{O}(t^4) \tag{10a}$$

$$(\mathbf{u}(t)-\mathbf{u}_0)\cdot\mathbf{q} = \mu_\delta\, t - \mu_r\,\mu_\delta\, t^2 + (\mu_r^2 - \mu^2/2)\,\mu_\delta\, t^3 + \mathcal{O}(t^4) \tag{10b}$$

where $\mu_\alpha = \mathbf{W}_\perp\cdot\mathbf{p} = \dot\alpha_{(t=t_0)}\,\cos\delta_0$, $\mu_\delta = \mathbf{W}_\perp\cdot\mathbf{q} = \dot\delta_{(t=t_0)}$, $\mu_r = W_r = v_r/r$ and $\mu^2 = \mu_\alpha^2+\mu_\delta^2$ (only the tangent plane components).

It is convenient for the following to rewrite Eqs. 10 in a slightly different form as,

$$(\mathbf{u}(t)-\mathbf{u}_0)\cdot\mathbf{p} = (1-\mu_r\, t)\,\mu_\alpha\, t + (\mu_r^2 - \mu^2/2)\,\mu_\alpha\, t^3 + \mathcal{O}(t^4) \tag{11a}$$

$$(\mathbf{u}(t)-\mathbf{u}_0)\cdot\mathbf{q} = (1-\mu_r\, t)\,\mu_\delta\, t + (\mu_r^2 - \mu^2/2)\,\mu_\delta\, t^3 + \mathcal{O}(t^4) \tag{11b}$$

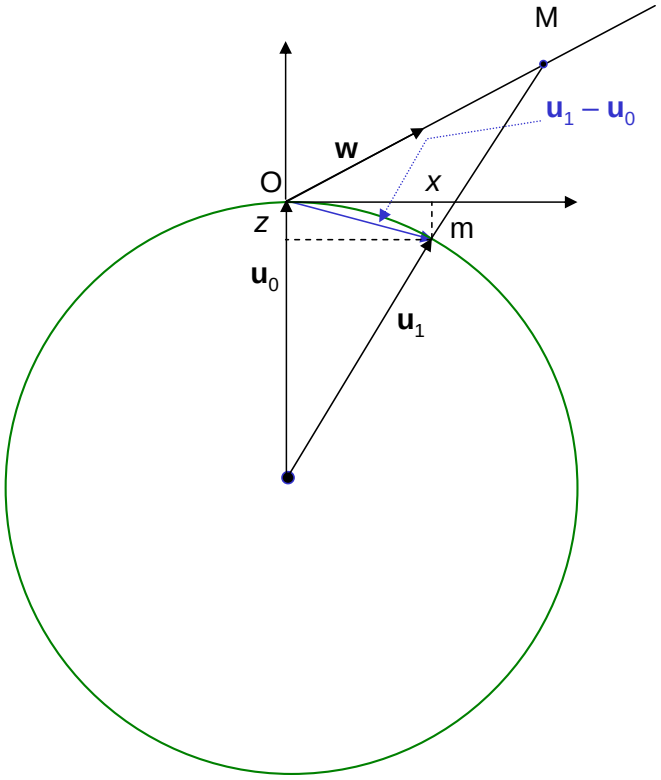


FIGURE 3: Relationship between the space motion $OM(t)$ and the apparent motion $Om(t)$ seen on the unit sphere. While $M$ and $m$ are related by a central projection, $m$ is linked to the coordinate $x$ by a parallel projection and so are the spherical coordinates of $m$ to the cartesian coordinates of $\mathbf{u}(t)-\mathbf{u}_0$.

The left-hand sides of (11) are just the two cartesian coordinates of $\mathbf{u}(t)-\mathbf{u}_0$ in the local frame

along $\mathbf{p}$ and $\mathbf{q}$ (Fig. 2) and this is then rewritten as,

$$x = (1 - \mu_r\, t)\, \mu_\alpha\, t + (\mu_r^2 - \mu^2/2)\, \mu_\alpha\, t^3 + \mathcal{O}(t^4) \tag{12a}$$

$$y = (1 - \mu_r\, t)\, \mu_\delta\, t + (\mu_r^2 - \mu^2/2)\, \mu_\delta\, t^3 + \mathcal{O}(t^4) \tag{12b}$$

which is the propagation model to third order in the plane of the sky. In this form this is the direct model yielding the star cartesian coordinates $(x, y)$ in the local frame at $t$ from the three components of the velocity vector $\mathbf{W}$ or, equivalently, that of the space proper motion $\mu_\alpha, \mu_\delta, \mu_r$. The goal now is to invert this model and to solve for $\mu_\alpha, \mu_\delta$ from the observed $x, y$, assuming $\mu_r$ to be a known quantity, or at least sufficiently well known for this purpose, given the uncertainties in $x$ and $y$.

It happens that the inversion to the third order is straightforward thanks to the factoring of the second order term with $(1 - \mu_r\, t)$.

$$\mu_\alpha\, t = \frac{1}{1 - \mu_r\, t} \left[ x - \left( \mu_r^2 t^2 - \frac{x^2 + y^2}{2} \right) x \right] \tag{13a}$$

$$\mu_\delta\, t = \frac{1}{1 - \mu_r\, t} \left[ y - \left( \mu_r^2 t^2 - \frac{x^2 + y^2}{2} \right) y \right] \tag{13b}$$

Then by expanding the first factor in power of $\mu_r\, t$ one has the good surprise to end up with very simple expressions as the terms in $t^2$ cancel out,

$$\mu_\alpha\, t = x(1 + \mu_r\, t) + \frac{x^2 + y^2}{2}\, x \tag{14a}$$

$$\mu_\delta\, t = y(1 + \mu_r\, t) + \frac{x^2 + y^2}{2}\, y \tag{14b}$$

### 3.3.1 Orders of magnitude

One considers a fast moving nearby star, with $V_r \sim V_\perp = 50$ km/s and a distance of 2 pc. This gives $W = V/r \sim 5''$/yr or 25 $\mu$rad/yr. The magnitudes of the different orders are given in Table 2. For the combination of Hipparcos and Gaia preliminary solution, the third order term is not required. However we will see below that this is not perfectly true for stars in the polar regions.

## 3.4 Relation to spherical coordinates

What is missing at this stage is the change of the spherical coordinates $\alpha - \alpha_0$ and $\delta - \delta_0$ between the two positions of the star. This is needed to relate the components of the proper motion to the observable quantities $\Delta\alpha\, \cos\delta_0$ and $\Delta\delta$. In the predictor mode, or explicit mode, the propagation model, allows to compute the position of the star at $t$ once the three components of the

TABLE 2: Orders of magnitude for the proper motion modelling for a star at 2pc with a velocity of 50 km/s.

| **Term in W** | **Amplitude** | $t^k$ | Over 20 years |
|---|---|---|---|
| $W$ | 5″/yr | $t$ | 100 ″ |
| $W^2$ | 125 $\mu$as/yr$^2$ | $t^2$ | 50 mas |
| $W^3$ | $3 \times 10^{-3}$ $\mu$as/yr$^3$ | $t^3$ | 25 $\mu$as |

proper motion are known. In the inverse mode, and using only two positions at two epochs, one can inverse (11) and solve for $\mu_\alpha$ and $\mu_\delta$, provided $\mu_r$ is known. With more observations, and this is not the purpose of the HTM project, the three components could be retrieved, meaning the radial velocity could be extracted from astrometric measurements without spectroscopy, or form other combinations with two independent determinations of proper motions as shown by Dravins and co-workers (Dravins et al. (1999)). This is clearly a work to be done later with the complete Gaia solution of the Hipparcos stars.

As said earlier, $x, y$ in (12) are the cartesian coordinates at $t$ in the tangent plane of the star direction relative to its direction at $t = 0$. The point of coordinates $x, y$ in that plane is related to the star direction on the unit sphere by a parallel projection (named orthographic projection by map makers) from the sphere to the plane. This projection should not be mistaken for the more usual projection used in photographic plate astronomy which is a central or gnomonic projection. The two are very similar, identical to second order, but not to higher orders. The difference is clearly shown in Fig. 4, with the gnomonic projection on the left and the orthographic projection on the right. The central projection is the imaging realised by an ideal optical instrument mapping a region of the celestial sphere on a plane, while the parallel projection is how we see a planetary surface at large distance. For the purpose of comparison, I have derived the relevant trigonometric formulas to third order of the small displacement for each of the two projections. The details can be found respectively in Appendix A and B.

Inserting equations (37) in (14) yields the expressions of the proper motion components $\mu_\alpha, \mu_\delta$ as a function of the observed displacement between two epochs and of $\mu_r$. The algebra is straightforward and gives,

$$\begin{aligned} \mu_\alpha\, t = {} & \Delta\alpha^\star \\ & + \Delta\alpha^\star\, \mu_r\, t - \tan\delta_0\, \Delta\alpha^\star\, \Delta\delta \\ & + \frac{3\cos^2\delta_0 - 1}{6\,\cos^2\delta_0}\,(\Delta\alpha^\star)^3 - \tan\delta_0\, \Delta\alpha^\star\, \Delta\delta\, \mu_r t \end{aligned} \tag{15}$$

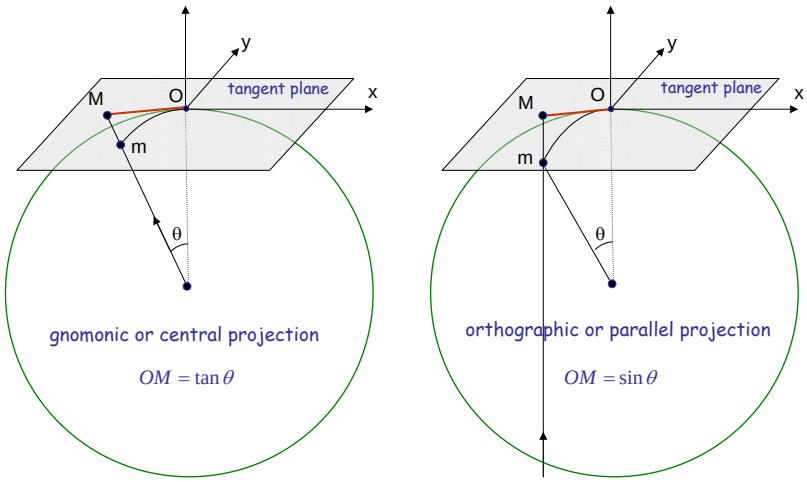


FIGURE 4: Comparison of the central (gnomonic) and parallel (orthographic) projections. The former corresponds to the standard photographic plate projection used in photographic or CCD astrometry. The latter is relevant here to deal with the link between the spatial motion in 3-D and the change of spherical coordinates. The two projections are identical to second order of $|\mathbf{OM}|$ but not to higher orders.

$$\begin{aligned}\mu_\delta\, t = {} & \Delta\delta \\ & + \Delta\delta\, \mu_r\, t + \frac{1}{2}\tan\delta_0\, (\Delta\alpha^\star)^2 \\ & + \frac{2\cos^2\delta_0 - 1}{2\,\cos^2\delta_0}\,(\Delta\alpha^\star)^2\,\Delta\delta + \frac{1}{2}\tan\delta_0\,(\Delta\alpha^\star)^2\,\mu_r t + \frac{\Delta\delta^3}{3}\end{aligned} \tag{16}$$

where the first, second and third order terms appear on different lines. In the following section numerical comparisons are done over the different orders. Equations (15) and (16) are probably given here for the first time (or better said, I know of no reference for them), since this level of approximation has never been needed in the past. They are sufficiently important to justify a second and truly independent derivation which is given in Appendix C, which leads to the same result and then supports my earlier using of the parallel projection.

Although I have reached now the goal set in the start of this section, one can take advantage of the formulas obtained in the parallel projection, to write down the predictor model to the third order of the proper motion. A parametric form is given with the set of equations (12) giving $x, y$ as a function of the three components of the proper motion (including the radial one) and then equations (38) giving $\Delta\alpha\,\cos\delta_0$ and $\Delta\delta$ as a function of $x, y$. Numerically, this solves the problem at this level of approximation. Now combining these equations together allows one to eliminate the $x$ and $y$ and obtain explicit expressions to compute $\Delta\alpha\,\cos\delta_0$ and $\Delta\delta$ at $t$. This is just an algebraic substitution which yields up to $t^3$ to,

$$\begin{aligned}\Delta\alpha\cos\delta_0 &= \mu_\alpha\, t \\ &\quad - \left[\mu_r\,\mu_\alpha - \tan\delta_0\,\mu_\alpha\,\mu_\delta\right]\, t^2 \\ &\quad + \left[\mu_r^2\,\mu_\alpha - 2\tan\delta_0\,\mu_r\,\mu_\alpha\,\mu_\delta + \tan^2\delta\,\mu_\alpha\,\mu_\delta^2 - \frac{\mu_\alpha^3}{3\,\cos^2\delta_0}\right]\, t^3\end{aligned} \tag{17}$$

$$\begin{aligned}\Delta\delta &= \mu_\delta\, t \\ &\quad - \left[\mu_r\,\mu_\delta + \frac{\tan\delta_0}{2}\,\mu_\alpha^2\right]\, t^2 \\ &\quad + \left[\mu_r^2\,\mu_\delta + \tan\delta_0\,\mu_r\,\mu_\alpha^2 - \frac{\mu_\alpha^2\,\mu_\delta}{2\,\cos^2\delta_0} - \frac{\mu_\delta^3}{3}\right]\, t^3\end{aligned} \tag{18}$$

Again exactly the same expressions are obtained by the alternate derivation given in Appendix C.

## 3.5 Inversion of the full model

In the numerical applications I use also the inversion of the full model by numerical methods, which suits perfectly the needs of the HTPM project, but without the insight provided by the analytical inversions. Equations (4) or (5) can be seen as explicit expressions like,

$$\alpha(t) = F_\alpha(\alpha_0, \delta_0, \mu_\alpha, \mu_\delta, \mu_r, t) \tag{19a}$$

$$\delta(t) = F_\delta(\alpha_0, \delta_0, \mu_\alpha, \mu_\delta, \mu_r, t) \tag{19b}$$

to compute the right ascension and declination of the star at any time from the kinematical model. Taken as functions of $\mu_\alpha, \mu_\delta$ these are two non-linear equations that can be solved for these quantities when all the other parameters are known. Numerically the solution can be obtained with a Newton-Raphson fixed point iteration starting with the initial values,

$$\mu_\alpha = \Delta\alpha\,\cos\delta_0/t \tag{20a}$$

$$\mu_\delta = \Delta\delta/t \tag{20b}$$

and then solving repeatedly the linear system for $(\mu_\alpha)_n$ and $(\mu_\delta)_n$,

$$\alpha(t) - \alpha_{n-1}(t) = \frac{\partial F_\alpha}{\partial\mu_\alpha}\left[(\mu_\alpha)_n - (\mu_\alpha)_{n-1}\right] + \frac{\partial F_\alpha}{\partial\mu_\delta}\left[(\mu_\delta)_n - (\mu_\delta)_{n-1}\right] \tag{21a}$$

$$\delta(t) - \delta_{n-1}(t) = \frac{\partial F_\delta}{\partial\mu_\alpha}\left[(\mu_\alpha)_n - (\mu_\alpha)_{n-1}\right] + \frac{\partial F_\delta}{\partial\mu_\delta}\left[(\mu_\delta)_n - (\mu_\delta)_{n-1}\right] \tag{21b}$$

where $n$ is the iteration number and $\alpha_{n-1}(t), \delta_{n-1}(t)$ are computed with (19) with $(\mu_\alpha)_{n-1}$ and $(\mu_\delta)_{n-1}$, the solution of the inversion at the $(n-1)$th iteration. The convergence is quadratic and only two or three are needed to reach the computer numerical precision. In practice one works always with $(\alpha(t) - \alpha_0)\ \cos\delta_0$ and $\delta(t) - \delta_0$ by changing the definition of $F_\alpha$ and $F_\delta$ accordingly. This has been implemented into a small fortran subroutine and the partial derivatives are numerically evaluated at each iteration.

# 4 Numerical illustrations

A fairly simple simulation has been created to check and illustrate the validity of the different inversion models in the evaluation of the proper motion components when the positions are known at two epochs. The goal is (i) to test the errors resulting from the truncation of the models to first, second or third order, by comparison to the exact solution and (ii) to assess its sensitivity to an approximate knowledge of the radial proper motion $\mu_r$. Since this will affect only nearby stars from which Hipparcos parallaxes are known to one or two percent, the radial velocity is the most likely source of uncertainty in $\mu_r$ for the HTPM project.

A set of stars is generated at different declinations, with specified values for the proper motion in $\alpha$ and $\delta$, for the parallax and for the radial velocity, together with a time interval between the two epochs. As no problems are expected for the distant and slow moving stars, the tests concentrate only on the the nearby stars, where the model truncation should be the most visible. A run consists of computing the position at the second epoch with the full kinematical model given in equation (5), and then solve for the proper motion with the different models, using the true $\Delta\alpha\cos\delta_0$ and $\Delta\delta$ as input. In the first set of tests, the $\mu_r$ value used for the processing is the same as the one used for the simulation, while an offset is applied in other runs, to simulate a poor knowledge. Results are presented in a series of table with similar layout, but the units used in the columns may change from table to table to adjust to the magnitude of the numbers. Units are always given in the columns headers. The caption of each table describes the content of the simulation and the goal of the test. The columns labelled first, second and third order refer to equations (15)-(16) and to the truncation level. The full inversion is the exact solution of the propagation equations of Sec. 3.5. Computations have been done in quadruple precision (128 bits for the reals) to avoid accuracy loss from differences between nearly identical numbers.

TABLE 3: Grid of simulations

| n | t<br>yr | $\varpi$<br>mas | $\mu_\alpha$<br>mas/yr | $\mu_\delta$<br>mas/yr | $V_r$<br>km/s | Noise<br>N or km/s |
|---|---|---|---|---|---|---|
| 1 | 100 | 500 | 2000 | 2000 | 50 | N |
| 2 | 20 | 500 | 2000 | 2000 | 50 | N |
| 3 | 20 | 50 | 100 | 100 | 50 | N |
| 4 | 20 | 500 | 2000 | 2000 | 50 | 5 km/s |
| 5 | 20 | 500 | 2000 | 2000 | 50 | 1 km/s |
| 6 | 20 | 500 | 2000 | 2000 | 20 | 2 km/s |
| 7 | 20 | 50 | 100 | 100 | 50 | 5 km/s |

TABLE 4: Determination of the proper motion components at the first epoch from positions at the first and second epochs, with a 100-year interval. The columns give the error between the computed and the true annual proper motion for each component. Reference parameters : $\varpi = 500$mas, $\mu_\alpha = \mu_\delta = 2000$mas/yr, $v_r = 50$km/s.

| $\delta$ | 1st order mas/yr | | 2nd order $\mu$as/yr | | 3rd order 0.001$\mu$as/yr | | full inversion 0.001$\mu$as/yr | |
|---|---|---|---|---|---|---|---|---|
| $^\circ$ | $\mu_\alpha$ | $\mu_\delta$ | $\mu_\alpha$ | $\mu_\delta$ | $\mu_\alpha$ | $\mu_\delta$ | $\mu_\alpha$ | $\mu_\delta$ |
| 85.0 | 17.1 | -16.3 | 97.7 | 94.0 | -333.0 | 435.4 | 0.00 | 0.00 |
| 75.0 | 2.1 | -8.7 | 22.2 | 2.3 | 1.7 | 35.4 | 0.00 | 0.00 |
| 60.0 | -1.8 | -6.8 | 8.9 | -3.0 | 2.9 | 4.5 | 0.00 | 0.00 |
| 45.0 | -3.2 | -6.1 | 4.6 | -3.1 | 1.0 | -1.0 | 0.00 | 0.00 |
| 30.0 | -4.0 | -5.7 | 2.3 | -2.7 | -0.2 | -2.9 | 0.00 | 0.00 |
| 15.0 | -4.6 | -5.4 | 0.7 | -2.2 | -1.0 | -3.7 | 0.00 | 0.00 |
| 0.0 | -5.1 | -5.1 | -0.6 | -1.6 | -1.6 | -4.0 | 0.00 | 0.00 |
| -15.0 | -5.6 | -4.8 | -1.9 | -0.8 | -2.1 | -3.9 | 0.00 | 0.00 |
| -30.0 | -6.2 | -4.5 | -3.4 | 0.2 | -2.5 | -3.5 | 0.00 | 0.00 |
| -45.0 | -7.0 | -4.1 | -5.2 | 1.8 | -2.6 | -2.2 | 0.00 | 0.00 |
| -60.0 | -8.4 | -3.4 | -8.2 | 5.5 | -1.3 | 1.9 | 0.00 | 0.00 |
| -75.0 | -12.3 | -1.5 | -14.7 | 20.5 | 17.1 | 23.2 | 0.00 | 0.00 |
| -85.0 | -27.0 | 5.8 | -16.9 | 146.1 | 513.0 | 187.7 | 0.00 | 0.00 |

The most extreme case (not to be met in practice), with nearby and high-velocity stars with a 100-year timespan. One shows clearly the importance of the second order terms in the propagation modelling, the near exact solution with third order terms, with the exception of the polar zones. The exact numerical solution converges everywhere.

TABLE 5: Determination of the proper motion components at the first epoch from positions at the first and second epochs, with a 20-year interval. The columns give the error between the computed and the true annual proper motion for each component. Reference parameters : $\varpi = 500$mas, $\mu_\alpha = \mu_\delta = 2000$mas/yr, $v_r = 50$km/s.

| $\delta$ | 1st order mas/yr | | 2nd order $\mu$as/yr | | 3rd order 0.001$\mu$as/yr | | full inversion 0.001$\mu$as/yr | |
|---|---|---|---|---|---|---|---|---|
| $^\circ$ | $\mu_\alpha$ | $\mu_\delta$ | $\mu_\alpha$ | $\mu_\delta$ | $\mu_\alpha$ | $\mu_\delta$ | $\mu_\alpha$ | $\mu_\delta$ |
| 85.0 | 3.4 | -3.2 | 3.9 | 3.7 | -2.6 | 3.4 | 0.00 | 0.00 |
| 75.0 | 0.4 | -1.7 | 0.9 | 0.1 | 0.0 | 0.3 | 0.00 | 0.00 |
| 60.0 | -0.4 | -1.4 | 0.4 | -0.1 | 0.0 | 0.0 | 0.00 | 0.00 |
| 45.0 | -0.6 | -1.2 | 0.2 | -0.1 | 0.0 | 0.0 | 0.00 | 0.00 |
| 30.0 | -0.8 | -1.1 | 0.1 | -0.1 | 0.0 | 0.0 | 0.00 | 0.00 |
| 15.0 | -0.9 | -1.1 | 0.0 | -0.1 | 0.0 | 0.0 | 0.00 | 0.00 |
| 0.0 | -1.0 | -1.0 | 0.0 | -0.1 | 0.0 | 0.0 | 0.00 | 0.00 |
| -15.0 | -1.1 | -1.0 | -0.1 | 0.0 | 0.0 | 0.0 | 0.00 | 0.00 |
| -30.0 | -1.2 | -0.9 | -0.1 | 0.0 | 0.0 | 0.0 | 0.00 | 0.00 |
| -45.0 | -1.4 | -0.8 | -0.2 | 0.1 | 0.0 | 0.0 | 0.00 | 0.00 |
| -60.0 | -1.7 | -0.7 | -0.3 | 0.2 | 0.0 | 0.0 | 0.00 | 0.00 |
| -75.0 | -2.5 | -0.3 | -0.6 | 0.8 | 0.1 | 0.2 | 0.00 | 0.00 |
| -85.0 | -5.4 | 1.2 | -0.7 | 6.0 | 4.2 | 1.5 | 0.00 | 0.00 |

Very nearby and high-velocity stars with a 20-year timespan, corresponding to the Hipparcos-Gaia case. One sees clearly the importance of the second order terms in the modelling, which meets the needs of the HTPM project everywhere. In practice the exact numerical solution is the method one should apply, given its performance and its fast convergence.

TABLE 6: Determination of the proper motion components at the first epoch from positions at the first and second epochs, with a 20-year interval. The columns give the error between the computed and the true annual proper motion for each component. Reference parameters are less extreme than in the previous tables : $\varpi = 50$mas, $\mu_\alpha = \mu_\delta = 100$mas/yr, $v_r = 50$km/s. **Warning**: first order column now in $\mu$as/yr instead of mas/yr and second in $0.001\mu$as/yr.

| $\delta$ | 1st order $\mu$as/yr | | 2nd order $0.001\mu$as/yr | | 3rd order $0.001\mu$as/yr | | full inversion $0.001\mu$as/yr | |
|---|---|---|---|---|---|---|---|---|
| $^\circ$ | $\mu_\alpha$ | $\mu_\delta$ | $\mu_\alpha$ | $\mu_\delta$ | $\mu_\alpha$ | $\mu_\delta$ | $\mu_\alpha$ | $\mu_\delta$ |
| 85.0 | 6.0 | -10.7 | 0.8 | 0.3 | 0.0 | 0.0 | 0.00 | 0.00 |
| 75.0 | -1.5 | -6.9 | 0.2 | 0.0 | 0.0 | 0.0 | 0.00 | 0.00 |
| 60.0 | -3.4 | -6.0 | 0.1 | 0.0 | 0.0 | 0.0 | 0.00 | 0.00 |
| 45.0 | -4.1 | -5.6 | 0.0 | 0.0 | 0.0 | 0.0 | 0.00 | 0.00 |
| 30.0 | -4.6 | -5.4 | 0.0 | 0.0 | 0.0 | 0.0 | 0.00 | 0.00 |
| 15.0 | -4.9 | -5.2 | 0.0 | 0.0 | 0.0 | 0.0 | 0.00 | 0.00 |
| 0.0 | -5.1 | -5.1 | 0.0 | 0.0 | 0.0 | 0.0 | 0.00 | 0.00 |
| -15.0 | -5.4 | -5.0 | 0.0 | 0.0 | 0.0 | 0.0 | 0.00 | 0.00 |
| -30.0 | -5.7 | -4.8 | 0.0 | 0.0 | 0.0 | 0.0 | 0.00 | 0.00 |
| -45.0 | -6.1 | -4.6 | -0.1 | 0.0 | 0.0 | 0.0 | 0.00 | 0.00 |
| -60.0 | -6.8 | -4.3 | -0.1 | 0.1 | 0.0 | 0.0 | 0.00 | 0.00 |
| -75.0 | -8.7 | -3.3 | -0.2 | 0.1 | 0.0 | 0.0 | 0.00 | 0.00 |
| -85.0 | -16.2 | 0.4 | -0.4 | 0.9 | 0.0 | 0.0 | 0.00 | 0.00 |

A representative intermediate Hipparcos star with a 20-year timespan, corresponding to the Hipparcos-Gaia case. Second order terms are needed to retrieve the proper motion without modelling error. In practice the exact numerical solution is the method one should apply.

TABLE 7: Determination of the proper motion components at the first epoch from positions at the first and second epochs, with a 20-year interval when the radial velocity used in the processing is wrong by 5km/s. The columns give the error between the computed and the true annual proper motion for each component. Reference parameters for the simulation : $\varpi = 500$mas, $\mu_\alpha = \mu_\delta = 2000$mas/yr, $v_r = 50$km/s, but $v_r = 55$km/s used in the analysis. **Warning**: all columns now in mas/yr

| $\delta$ | 1st order mas/yr | | 2nd order mas/yr | | 3rd order mas/yr | | full inversion mas/yr | |
|---|---|---|---|---|---|---|---|---|
| $^\circ$ | $\mu_\alpha$ | $\mu_\delta$ | $\mu_\alpha$ | $\mu_\delta$ | $\mu_\alpha$ | $\mu_\delta$ | $\mu_\alpha$ | $\mu_\delta$ |
| 85.0 | 3.4 | -3.2 | 0.1 | 0.1 | 0.1 | 0.1 | 0.10 | 0.10 |
| 75.0 | 0.4 | -1.7 | 0.1 | 0.1 | 0.1 | 0.1 | 0.10 | 0.10 |
| 60.0 | -0.4 | -1.4 | 0.1 | 0.1 | 0.1 | 0.1 | 0.10 | 0.10 |
| 45.0 | -0.6 | -1.2 | 0.1 | 0.1 | 0.1 | 0.1 | 0.10 | 0.10 |
| 30.0 | -0.8 | -1.1 | 0.1 | 0.1 | 0.1 | 0.1 | 0.10 | 0.10 |
| 15.0 | -0.9 | -1.1 | 0.1 | 0.1 | 0.1 | 0.1 | 0.10 | 0.10 |
| 0.0 | -1.0 | -1.0 | 0.1 | 0.1 | 0.1 | 0.1 | 0.10 | 0.10 |
| -15.0 | -1.1 | -1.0 | 0.1 | 0.1 | 0.1 | 0.1 | 0.10 | 0.10 |
| -30.0 | -1.2 | -0.9 | 0.1 | 0.1 | 0.1 | 0.1 | 0.10 | 0.10 |
| -45.0 | -1.4 | -0.8 | 0.1 | 0.1 | 0.1 | 0.1 | 0.10 | 0.10 |
| -60.0 | -1.7 | -0.7 | 0.1 | 0.1 | 0.1 | 0.1 | 0.10 | 0.10 |
| -75.0 | -2.5 | -0.3 | 0.1 | 0.1 | 0.1 | 0.1 | 0.10 | 0.10 |
| -85.0 | -5.4 | 1.2 | 0.1 | 0.1 | 0.1 | 0.1 | 0.10 | 0.10 |

Very nearby and high-velocity stars with a 20-year timespan, corresponding to the Hipparcos-Gaia case. In this case a noise is added to account for the approximate knowledge of the radial velocity. There is a 10% error, amounting here to 5 km/s. The first order model error is larger than the error resulting from the radial velocity and is similar to 2nd simulation above. Then in all other cases, the final error is about 100 $\mu$as/yr in the proper motion. For these rather extreme stars, the error in $v_r$ could be the major source of uncertainty in the determination of the Hipparcos proper motions using Gaia positions.

TABLE 8: Determination of the proper motion components at the first epoch from positions at the first and second epochs, with a 20-year interval when the radial velocity used in the processing is wrong by 1km/s. The columns give the error between the computed and the true annual proper motion for each component. Reference parameters for the simulation : $\varpi = 500$mas, $\mu_\alpha = \mu_\delta = 2000$mas/yr, $v_r = 50$km/s, but $v_r = 51$km/s used in the analysis. **Warning**: first column in mas/yr, others in $\mu$as/yr.

| $\delta$ | 1st order mas/yr | | 2nd order $\mu$as/yr | | 3rd order $\mu$as/yr | | full inversion $\mu$as/yr | |
|---|---|---|---|---|---|---|---|---|
| $^\circ$ | $\mu_\alpha$ | $\mu_\delta$ | $\mu_\alpha$ | $\mu_\delta$ | $\mu_\alpha$ | $\mu_\delta$ | $\mu_\alpha$ | $\mu_\delta$ |
| 85.0 | 3.4 | -3.2 | 24.4 | 24.1 | 20.4 | 20.4 | 20.44 | 20.44 |
| 75.0 | 0.4 | -1.7 | 21.3 | 20.5 | 20.4 | 20.4 | 20.44 | 20.44 |
| 60.0 | -0.4 | -1.4 | 20.8 | 20.3 | 20.4 | 20.4 | 20.44 | 20.44 |
| 45.0 | -0.6 | -1.2 | 20.6 | 20.3 | 20.4 | 20.4 | 20.44 | 20.44 |
| 30.0 | -0.8 | -1.1 | 20.5 | 20.3 | 20.4 | 20.4 | 20.44 | 20.44 |
| 15.0 | -0.9 | -1.1 | 20.5 | 20.4 | 20.4 | 20.4 | 20.44 | 20.44 |
| 0.0 | -1.0 | -1.0 | 20.4 | 20.4 | 20.4 | 20.4 | 20.44 | 20.44 |
| -15.0 | -1.1 | -1.0 | 20.4 | 20.4 | 20.4 | 20.4 | 20.44 | 20.44 |
| -30.0 | -1.2 | -0.9 | 20.3 | 20.5 | 20.4 | 20.4 | 20.44 | 20.44 |
| -45.0 | -1.4 | -0.8 | 20.2 | 20.5 | 20.4 | 20.4 | 20.44 | 20.44 |
| -60.0 | -1.7 | -0.7 | 20.1 | 20.7 | 20.4 | 20.4 | 20.44 | 20.44 |
| -75.0 | -2.5 | -0.3 | 19.8 | 21.3 | 20.4 | 20.4 | 20.44 | 20.44 |
| -85.0 | -5.4 | 1.2 | 19.7 | 26.4 | 20.4 | 20.4 | 20.44 | 20.44 |

Very nearby and high-velocity stars with a 20-year timespan, corresponding to the Hipparcos-Gaia case. In this case a noise is added to account for the approximate knowledge of the radial velocity. There is a 2% error, amounting here to 1 km/s. The first order model error is larger than the error resulting from the radial velocity and is similar to 2nd simulation above. Then in all other cases, the final error is about 20 $\mu$as/yr in the proper motion, and scales linearly with the error in $v_r$.

TABLE 9: Determination of the proper motion components at the first epoch from positions at the first and second epochs, with a 20-year interval when the radial velocity used in the processing is wrong by 1km/s. The columns give the error between the computed and the true annual proper motion for each component. Reference parameters for the simulation : $\varpi = 500$mas, $\mu_\alpha = \mu_\delta = 2000$mas/yr, $v_r = 20$km/s, but $v_r = 22$km/s used in the analysis. **Warning**: first column in mas/yr, others in $\mu$as/yr.

| $\delta$ | 1st order mas/yr | | 2nd order $\mu$as/yr | | 3rd order $\mu$as/yr | | full inversion $\mu$as/yr | |
|---|---|---|---|---|---|---|---|---|
| $^\circ$ | $\mu_\alpha$ | $\mu_\delta$ | $\mu_\alpha$ | $\mu_\delta$ | $\mu_\alpha$ | $\mu_\delta$ | $\mu_\alpha$ | $\mu_\delta$ |
| 85.0 | 4.0 | -2.6 | 43.5 | 45.3 | 40.9 | 40.9 | 40.90 | 40.90 |
| 75.0 | 1.0 | -1.1 | 41.4 | 41.2 | 40.9 | 40.9 | 40.90 | 40.90 |
| 60.0 | 0.3 | -0.7 | 41.1 | 40.9 | 40.9 | 40.9 | 40.90 | 40.90 |
| 45.0 | 0.0 | -0.6 | 41.0 | 40.8 | 40.9 | 40.9 | 40.90 | 40.90 |
| 30.0 | -0.2 | -0.5 | 40.9 | 40.8 | 40.9 | 40.9 | 40.90 | 40.90 |
| 15.0 | -0.3 | -0.5 | 40.9 | 40.8 | 40.9 | 40.9 | 40.90 | 40.90 |
| 0.0 | -0.4 | -0.4 | 40.9 | 40.8 | 40.9 | 40.9 | 40.90 | 40.90 |
| -15.0 | -0.5 | -0.4 | 40.9 | 40.9 | 40.9 | 40.9 | 40.90 | 40.90 |
| -30.0 | -0.6 | -0.3 | 40.8 | 40.9 | 40.9 | 40.9 | 40.90 | 40.90 |
| -45.0 | -0.8 | -0.2 | 40.8 | 40.9 | 40.9 | 40.9 | 40.90 | 40.90 |
| -60.0 | -1.1 | -0.1 | 40.8 | 41.0 | 40.9 | 40.9 | 40.90 | 40.90 |
| -75.0 | -1.9 | 0.3 | 40.7 | 41.5 | 40.9 | 40.9 | 40.90 | 40.90 |
| -85.0 | -4.8 | 1.8 | 41.5 | 46.2 | 40.9 | 40.9 | 40.90 | 40.90 |

Very nearby and high-velocity stars with a 20-year timespan, corresponding to the Hipparcos-Gaia case, but with $v_r = 20$km/s instead of 50 km/s in the preceding simulation. In this case a noise is added to account for the approximate knowledge of the radial velocity. There is an error of 2km/s. The first order model error is larger than the error resulting from the radial velocity and of the order of 1mas/yr. Then in all other cases, the final error is about 40 $\mu$as/yr in the proper motion, and scales linearly with $v_r$.

TABLE 10: Determination of the proper motion components at the first epoch from positions at the first and second epochs, with a 20-year interval when the radial velocity used in the processing is wrong by 5km/s. The columns give the error between the computed and the true annual proper motion for each component. Reference parameters for the simulation : $\varpi = 50$mas, $\mu_\alpha = \mu_\delta = 100$mas/yr, $v_r = 50$km/s, but $v_r = 55$km/s used in the analysis. **Warning**: all columns now in $\mu$as/yr

| $\delta$ | 1st order $\mu$as/yr | | 2nd order $\mu$as/yr | | 3rd order $\mu$as/yr | | full inversion $\mu$as/yr | |
|---|---|---|---|---|---|---|---|---|
| $^\circ$ | $\mu_\alpha$ | $\mu_\delta$ | $\mu_\alpha$ | $\mu_\delta$ | $\mu_\alpha$ | $\mu_\delta$ | $\mu_\alpha$ | $\mu_\delta$ |
| 85.0 | 6.0 | -10.7 | 0.5 | 0.5 | 0.5 | 0.5 | 0.51 | 0.51 |
| 75.0 | -1.5 | -6.9 | 0.5 | 0.5 | 0.5 | 0.5 | 0.51 | 0.51 |
| 60.0 | -3.4 | -6.0 | 0.5 | 0.5 | 0.5 | 0.5 | 0.51 | 0.51 |
| 45.0 | -4.1 | -5.6 | 0.5 | 0.5 | 0.5 | 0.5 | 0.51 | 0.51 |
| 30.0 | -4.6 | -5.4 | 0.5 | 0.5 | 0.5 | 0.5 | 0.51 | 0.51 |
| 15.0 | -4.9 | -5.2 | 0.5 | 0.5 | 0.5 | 0.5 | 0.51 | 0.51 |
| 0.0 | -5.1 | -5.1 | 0.5 | 0.5 | 0.5 | 0.5 | 0.51 | 0.51 |
| -15.0 | -5.4 | -5.0 | 0.5 | 0.5 | 0.5 | 0.5 | 0.51 | 0.51 |
| -30.0 | -5.7 | -4.8 | 0.5 | 0.5 | 0.5 | 0.5 | 0.51 | 0.51 |
| -45.0 | -6.1 | -4.6 | 0.5 | 0.5 | 0.5 | 0.5 | 0.51 | 0.51 |
| -60.0 | -6.8 | -4.3 | 0.5 | 0.5 | 0.5 | 0.5 | 0.51 | 0.51 |
| -75.0 | -8.7 | -3.3 | 0.5 | 0.5 | 0.5 | 0.5 | 0.51 | 0.51 |
| -85.0 | -16.2 | 0.4 | 0.5 | 0.5 | 0.5 | 0.5 | 0.51 | 0.51 |

Representative Hipparcos stars, not too nearby and with moderate proper motion, with a 20-year timespan, corresponding to the Hipparcos-Gaia case. In this case a noise is added to account for the approximate knowledge of the radial velocity. There is a 10% error, amounting here to 5 km/s. The first order model error is larger than the error resulting from the radial velocity and is similar to 3nd simulation above and remains below the 10$\mu$as/yr almost everywhere. Then in all other cases, the final error is about 0.5 $\mu$as/yr in the proper motion, meaning the precise knowledge of radial velocity won't be a source of concern for most of the Hipparcos stars.

# Part II

# Application to the HTPM project

## 5 Introduction to Part II

In this part I apply the propagation model and its inversion to the determination of the proper motions for Hipparcos stars, using the Hipparcos position in 1991.25 and an early determination of position with Gaia around 2012.25. The goal is to confirm with an extensive simulation the quick insight regarding the achievable performances, which should be of the order of $1-2$ mas/20 yr $\sim 50-100$ $\mu$as/yr. The Hipparcos positions at the first epoch have a typical $\sim 1$ mas accuracy, and the determination of the Gaia barycentric position with only six month of data will have its uncertainty primarily determined by the Hipparcos parallax accuracy. With observations at two Gaia epochs or more, this should be below 1 mas, but not much below this value. This is the purpose of the simulation to have a realistic sampling of the observations and to solve for the barycentric position with a 2-parameter solution $(\alpha, \delta)$, using the Hipparcos parallaxes and proper motions in the observation modelling. From this solution for each Hipparcos star observable by Gaia ($> 6$ mag) the new proper motion is computed as explained in the first part of this note and compared to the true value used to generate the observations. Various plots are produced to show the statistical error distribution, its pattern as a function of the position and the impact of the inversion model on the number of outliers.

### 5.1 The simulation

The simulation generates Gaia observations of the Hipparcos stars over a duration of six months, using the nominal scanning law and a star catalogue built from Hipparcos. The main features of this simulation are shown in Fig. 5.

- There is one branch for the generation of noise-free observations from a perfect sky realised by propagating Hipparcos positions to the Gaia epoch using Hipparcos proper motion and then the parallax to generate the observations recorded by Gaia.

Given the importance of the radial velocity in this analysis, all Hipparcos stars have been given a radial velocity from a uniform distribution in $[-30, +30]$ km/s). They are used in the propagation model.

- A second branch produces the computed values based on a reference catalogue simulating the approximate sky known for the data processing. This catalogue is generated by adding random errors to the Hipparcos astrometric parameters and to the radial velocity as well. For the position and parallax I have used the standard errors of the Hipparcos catalogue to generate the errors, while a constant $\sigma_\mu = 2\mu$as/yr have been used for each component of the proper motion. For the radial velocity most of the runs have been made with a random error in the radial velocity of standard deviation 2km/s.

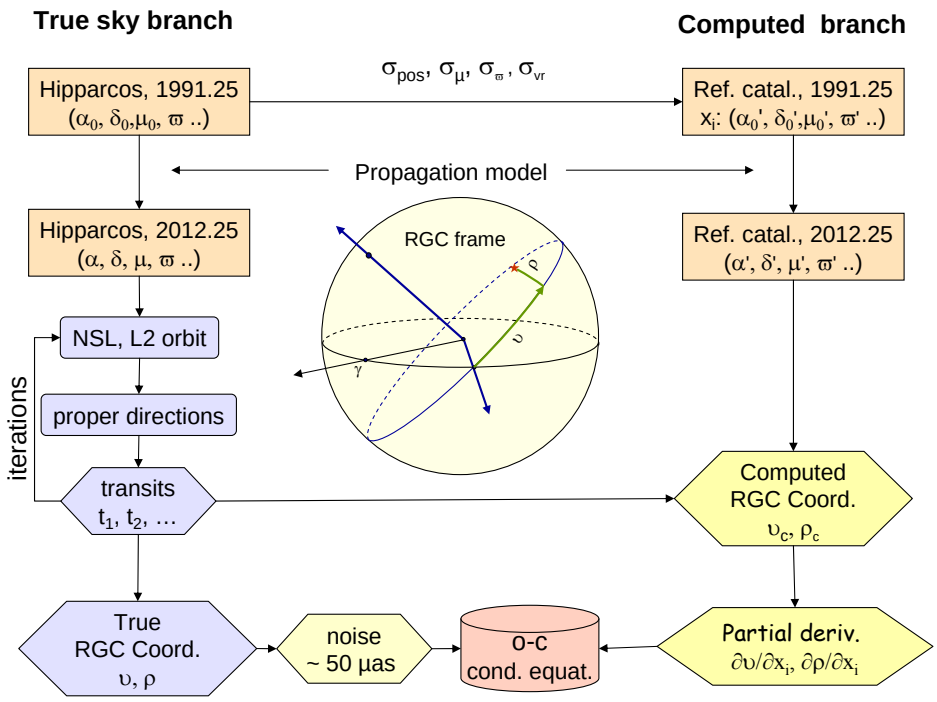


FIGURE 5: Flow chart of the simulation, with the observation branch on the left and the computed branch on the right. The scan reference frame is shown in the inset.

At the end of the computed branch one also evaluates the partial derivatives of the computed field coordinates with respect to each of the five astrometric parameters. Although I am only concerned with the positions for the HTPM project, tests have been run to solve for the five parameters over 5 years, in order to check the implementation with noiseless and noisy data.

The expressions noisy or noiseless do not refer to the observation noise used to create Gaia-like observations, which is very small for bright stars compared to the uncertainty in the Hipparcos positions, but to the offset between the reference catalogue and the simulated sky used to solve for the Gaia barycentric positions. This reference catalogue is the source of the reference parallaxes and proper motions used to correct the accurate apparent directions observed by Gaia for the parallactic shift and to bring all observations collected during the first six months to a single epoch, namely 2012.25.

In the presentation of the results below, the first set of plots deals with noiseless data, meaning processing the observations with a perfect knowledge of parallax and proper motions, and the accuracy is just limited by the Gaia observational noise of about 35-40$\mu$as along-scan for each field transit, and 5 times larger across scan (JDB-053).

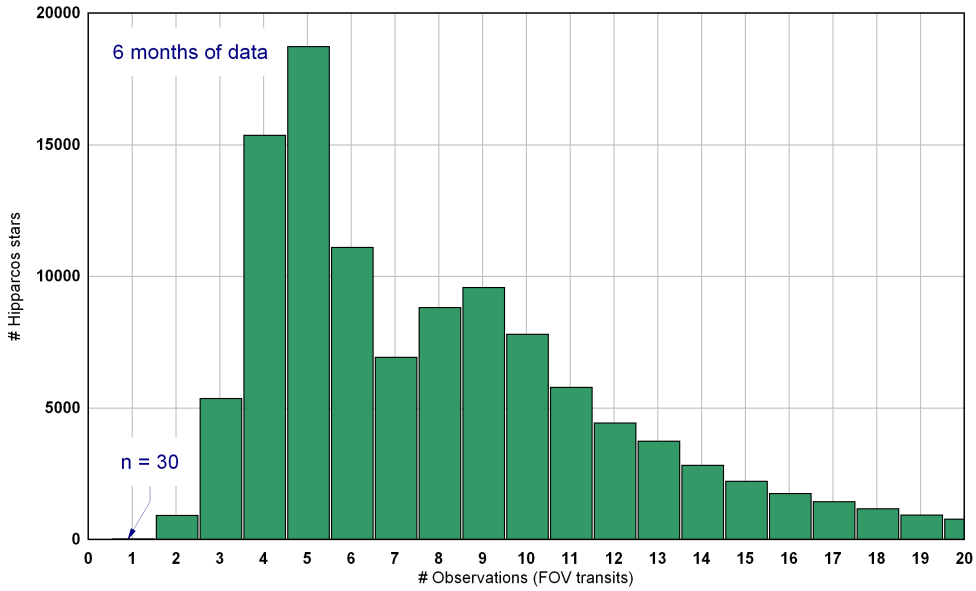


FIGURE 6: Distribution of the number of field transits for the Hipparcos stars over a period of six months.

There are in the Hipparcos Catalogue $\sim$ 113, 500 stars fainter than $H = 6$ (meaning 4500 brighter than this limit on the sky). Figs. 6 and 7 give respectively the histograms of the number of FOV transits and epochs over 6 months for the simulation catalogue of 113, 500 stars. A new epoch starts when the interval between two successive observations is larger than 2 days. In fact, when this happens, the interval is in general much larger, between 3 to 6 weeks. Observations at two well separated epochs (two different scan directions) are needed to solve for the star position using primarily the along-scan information. While the Gaia astrometric accuracy at the transit level is not very important for the HTPM project, the distribution of the scanning directions matters and this is directly connected to the number of epochs.

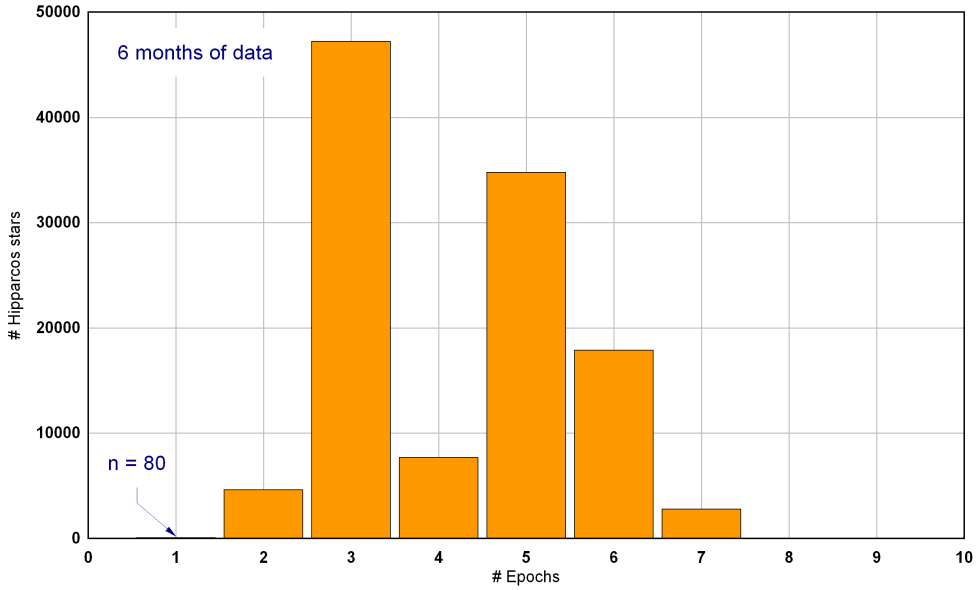


FIGURE 7: Distribution of the number of epochs at which the Hipparcos stars are observed during a period of six months.

During the processing, some stars were removed when the observation equations were found ill-conditioned, leading to too strong correlations between $\alpha$ and $\delta$ or singular values when solving for the position. To avoid lengthy discussions on limiting cases, I have removed all stars with less than 4 transits or less than two epochs, although many of them might have ended up with acceptable solution. Likewise the stars with poor astrometric accuracy ($\sigma_\varpi > 4$mas) in the Hipparcos Catalogue have not been included in the simulation, as not suitable to derive accurate proper motions. This left 103,500 stars in the final exploitation and in the solutions discussed in the following sections.

# 6 Results of the processing

## 6.1 Perfect reference catalogue

The Hipparcos catalogue of 1991.25 is propagated to 2012 to generate Gaia observations and the parallaxes and proper motions of the **same** catalogue are used to process the data, as if one had an exact knowledge of these two quantities. The tests are meant to check bias or modelling errors and are not relevant to determine the accuracy expected from a more realistic situation with an error on the parallax and annual proper motion of the order of 1 mas and 1mas/yr. The noise comes just from the Gaia photon noise on the along-scan and across-scan directions. Observations equations are weighed according to this noise, meaning AC observations are downweighed by a factor 25 relative to the AL observations. A different weighting scheme is adopted in Sect. 6.2 when the post-fit residuals originate essentially from the offset reference catalogue rather than photon noise.

The histograms of the errors in proper motion components are shown in Fig. 8 for $\mu_\alpha$ and Fig. 9 for $\mu_\delta$. The typical error is about $1\mu$as/yr, corresponding roughly to $\sigma_{\rm al}/\sqrt(n)/\tau$, with the number of transits over six months $n \simeq 8$, the timespan between the two epochs $\tau = 21$ years and $\sigma_{\rm al} = 40\,\mu$as. A small (between 1 and 2) multiplying geometric factor must be applied to account for the orientation of the scan relative to the local frame.

The next two plots are designed to show the outliers in the distributions for the same ideal conditions with a perfect reference catalogue. Fig. 10 shows for each star the error (computed - true value) for the proper motion in RA (blue) and declination (red) in $\mu$as/yr. There are very very few outliers, if any, among the $103,000$ data points, and the most extreme deviations can just result from a couple of truly exceptional values of noise produced by the random generator. I have not attempted to trace them back in detail.

The plot in Fig. 11 is one of the most interesting of the series. The conditions are the same as for Fig. 10, with the exception that the proper motion is computed from the two end-point observations with the first order model given by the first lines of equations (15)-(16). This is similar to the evaluation of the derivative of a function from its first differences. The scale of the plot has been extended to 100 $\mu$as/yr to show the number of outliers and the magnitude of the modelling errors on the nearest stars, when the inversion model is too crude. This can generate errors larger than 100$\mu$as/yr, much larger than those expected in the HTPM project when using a more realistic reference catalogue.

In this run a test is done on the radial velocity to assess the resulting error in the proper motion when no prior information is available on the stellar $v_r$. A value of $v_r$ has been used to simulate the observations, while $v_r = 0$ has been used in the processing. This will be the case for a good fraction of the Hipparcos entries, hopefully not the nearby stars. Fig. 12 gives the error (computed - true) in the proper motion components. Most of the 100,000 stars fall in the central

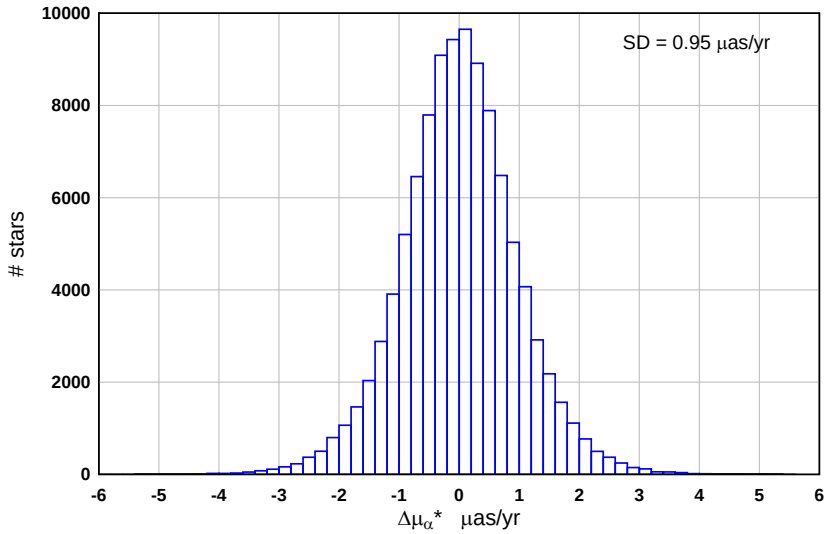


FIGURE 8: **Errors in right ascension**. Histogram showing the distribution of the errors (computed - true value) for the proper motion in right ascension for a perfect reference catalogue. The only noise comes from Gaia random photon noise at the level of 40 $\mu$as per transit on the along-scan direction. The exact inversion model is used to compute the proper motion from the positions at the two end epochs. The standard deviation of the distribution is $\sim 1\mu$as/yr as expected for $\sim 10$ observations and a 21-year timespan between the two epochs.

region with very small errors (perfect position catalogue used as reference), with few hundreds large outliers.

This can be accounted by the restriction of (15)-(16) to second order,

$$\mu_\alpha\, t = \Delta\alpha^\star + \Delta\alpha^\star\, \mu_r\, t - \tan\delta_0\, \Delta\alpha^\star\, \Delta\delta \tag{22a}$$

$$\mu_\delta\, t = \Delta\delta + \Delta\delta\, \mu_r\, t + \frac{1}{2}\tan\delta_0\, (\Delta\alpha^\star)^2 \tag{22b}$$

By taking $v_r = 0$ there is a modelling error in the processing of $\Delta\alpha^\star\, \mu_r$ in $\mu_\alpha$ and $\Delta\delta\, \mu_r$ in $\mu_\delta$. This is directly proportional to the parallax, and the nearest stars are the most affected. This is outstanding in Fig. 13 when the errors are plotted as a function of the parallax. The effect starts being visible for $\varpi > 30$ mas and becomes really significant at 50 mas. This implies that for all these stars, it won't be possible to achieve the best accuracy permitted by the astrometric measurements if radial velocities are not available.

Among the Hipparcos stars, there are (rounded numbers),

- 200 with $\varpi > 100$ mas,

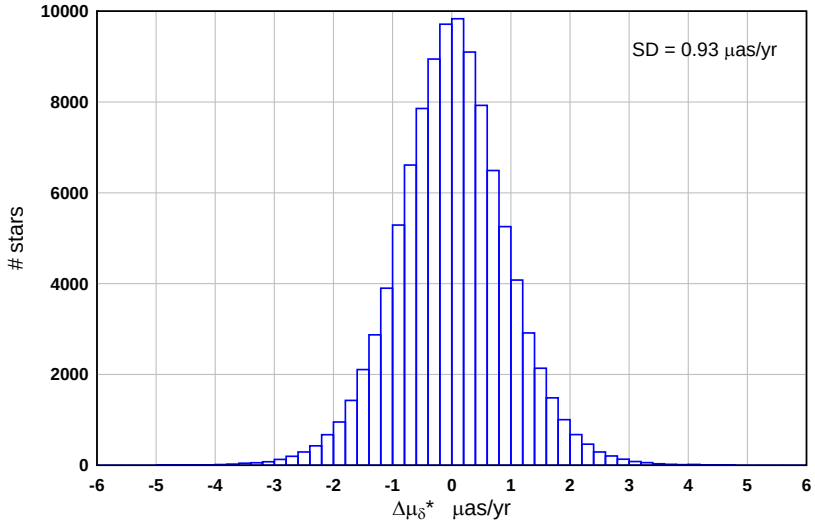


FIGURE 9: **Errors in declination**. Histogram showing the distribution of the errors (computed - true value) for the proper motion in declination for a perfect reference catalogue. The only noise comes from Gaia random photon noise at the level of 40 $\mu$as per transit on the along-scan direction. The exact inversion model is used to compute the proper motion from the positions at the two end epochs. The standard deviation of the distribution is $\sim 1\mu$as/yr as expected for $\sim 10$ observations and a 21-year timespan between the two epochs.

- 900 with $\varpi > 50$ mas,
- 1500 with $\varpi > 40$ mas,
- 3000 with $\varpi > 30$ mas.

I have not checked yet in detail how many $v_r$ are currently missing, but the Pulkovo Compilation of radial velocities contains this information for 35495 Hipparcos stars (Gontcharov (2006)), and one may expect that the nearest stars are all there. From visual inspection of the stars with parallaxes around 100 mas, this is almost the case. Since the error produced by this second order term, can be estimated as a function of the radial velocity, a factor can be published to update the HTPM proper motions when $v_r$ becomes known, or to correct them when better $v_r$ are known. This means that both the reference $v_r$ and $\varpi$ used in the model must be published with the proper motion list.

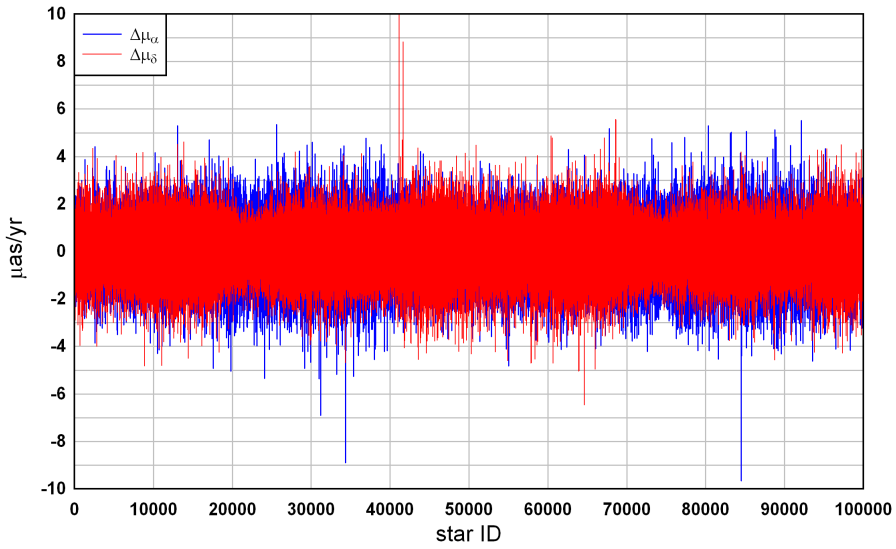


FIGURE 10: **Outliers in RA and dec**. Errors (computed - true value) for the proper motion in right ascension (blue) and declination (red) for a perfect reference catalogue. The only noise comes from Gaia random photon noise at the level of 40 $\mu$as per transit on the along-scan direction and the exact inversion model is used to compute the proper motion from the positions at the two end epochs.

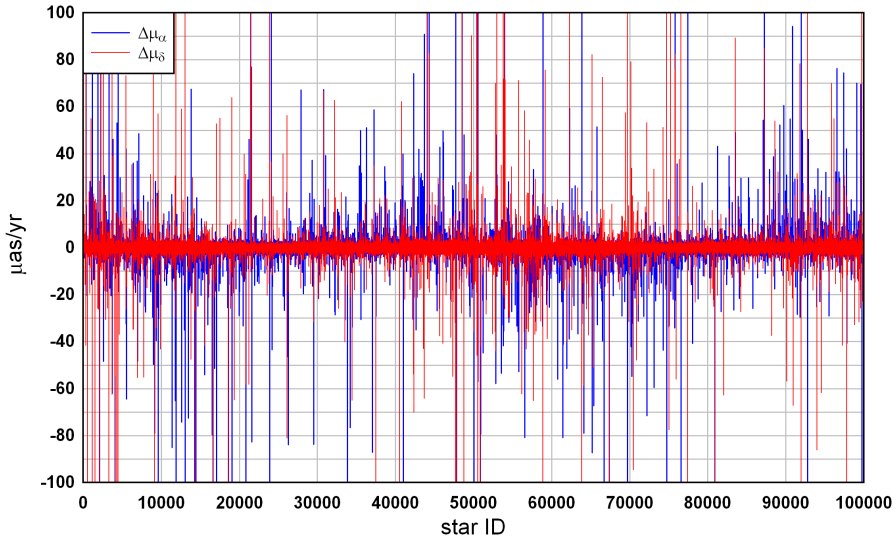


FIGURE 11: **Outliers from truncated model**. Errors (computed - true value) for the proper motion in right ascension (blue) and declination (red) for a perfect reference catalogue. The only statistical noise comes from Gaia random photon noise at the level of 40 $\mu$as per transit on the along-scan direction. A first order inversion model has been applied to evaluate the proper motion components from the positions at the two end epochs. The numerous outliers result from modelling errors and not from statistical noise and concern only the nearest stars.

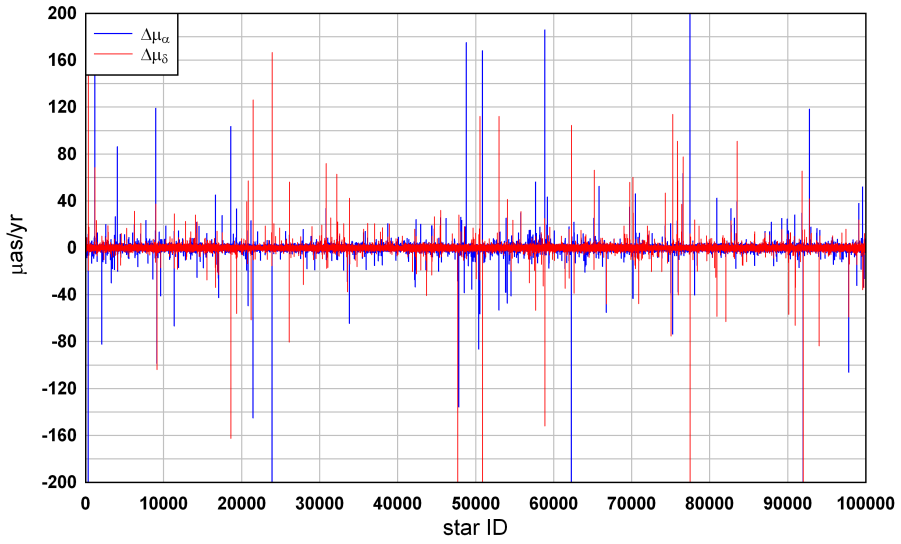


FIGURE 12: **Errors when using** $v_r = 0$. Errors (computed - true value) for the proper motion in right ascension (blue) and declination (red) for a perfect reference catalogue in position and parallax, but with unknown radial velocity, taken as $v_r = 0$ in the processing (and $v_r \neq 0$ to generate the observations).

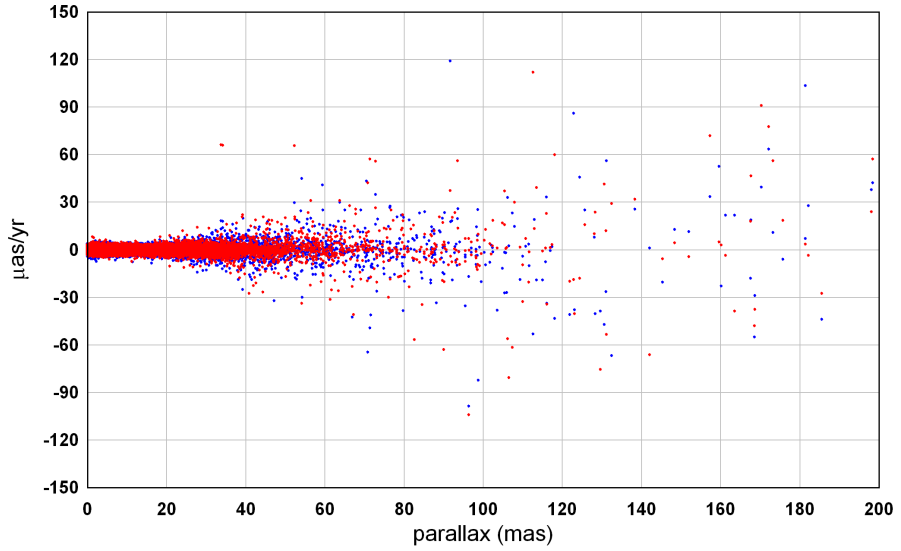


FIGURE 13: **Errors with parallaxes when using** $v_r = 0$. Errors (computed - true value) for the proper motion in right ascension (blue) and declination (red) as a function of the parallax for a perfect reference catalogue in position and parallax, but with unknown radial velocity, taken as $v_r = 0$ in the processing (and $v_r \neq 0$ to generate the observations).

## 6.2 Realistic data

Hereafter, the reference catalogue used now for the processing is randomly shifted from the reference sky using Hipparcos standard deviations as input of the gaussian random generator. As said earlier, this means that the reference positions at the first epoch are randomly shifted from the true sky position and that the parallaxes and proper motions used in the processing are also different from their true values.

### 6.2.1 Accuracy of the proper motions

The proper motions are computed by using the full inversion model (21) by combining the Gaia observations with the shifted Hipparcos positions (our best knowledge of the sky) in 1991.25. Trials with the second or third order models have also been made, with no difference in the results.

One compares for each star the proper motion obtained from the processing to the true value used to generate the observations. Therefore this is a true error and not a formal error based on residuals. The distributions of the errors in $\mu$as/yr are shown in Figs. 14 and 15 respectively for the right ascension and the declination. The two distributions are very regular and almost

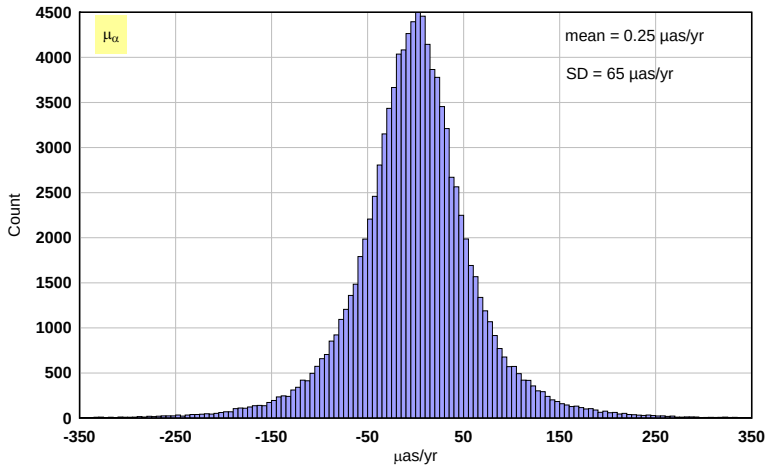


FIGURE 14: **Errors in right ascension**. Histogram showing the distribution of the errors (computed - true value) for the proper motion in right ascension. The standard deviation of the distribution is 65 $\mu$as/yr and there are tails slightly larger than a pure normal distribution, as expected since the accuracy is not constant over the sky.

symmetric with respect to the centre, with no statistically significant bias. The tails are not visible on this diagram, but they are very small. Outliers are shown and discussed in Sect. 6.2.2. The standard deviation of the distribution in right ascension is 65 $\mu$as/yr, and very stable against new seed in the random number generator. This is slightly better for declination with 48 $\mu$as/yr and this comes directly from a similar difference in the Hipparcos catalogue.

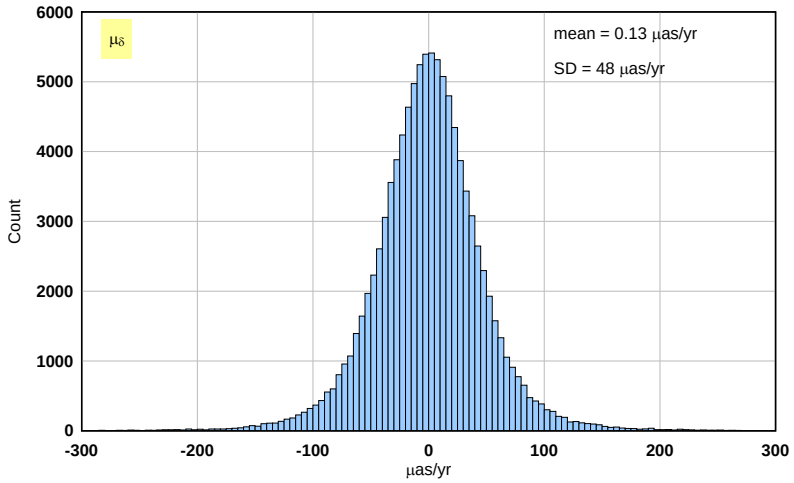


FIGURE 15: **Errors in declination**. Histogram showing the distribution of the errors (computed - true value) for the proper motion in declination. The standard deviation of the distribution is 48 $\mu$as/yr, with not significant tails larger than from a pure normal distribution.

The variation of the true errors with magnitude is shown in Fig. 16 as a smoothed representation of the standard deviations of the errors computed per bin of magnitude. The median of the catalogue is at $H = 8.5$, corresponding to an error of 53 and 40 $\mu$as/yr respectively in right ascension and declination.

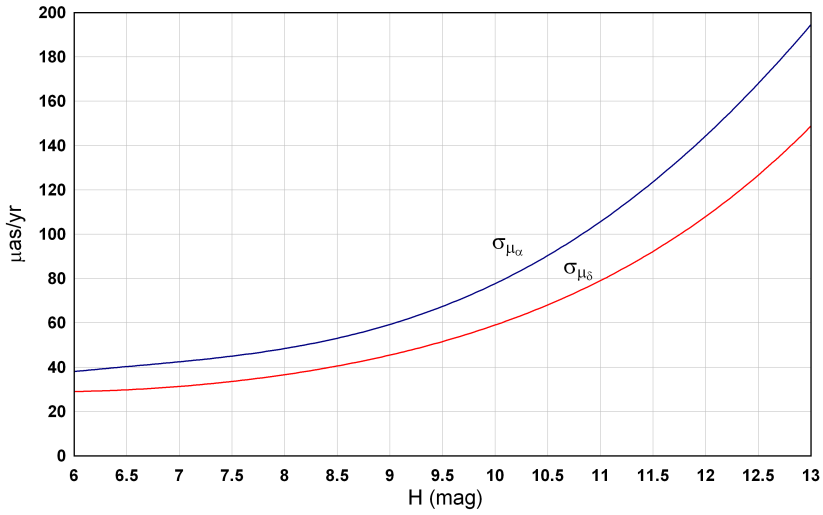


FIGURE 16: **Standard deviations vs. magnitude**. Standard deviations of the true error in the computation of the proper motion averaged over the sky as a function of the Hipparcos magnitude.

The last plot of this group gives the histogram of,

$$\delta|\boldsymbol{\mu}| = (\delta\mu_\alpha^2 + \delta\mu_\delta^2)^{1/2} \tag{23}$$

This is the yearly increase of the distance between the position propagated with the computed proper motions and the true position. This is not the same as the error in the modulus of the proper motion, but simply the modulus of the small vector between the true and the computed yearly motion on the sky. The distribution appears is Fig. 17, and is very close to a Rayleigh distribution.

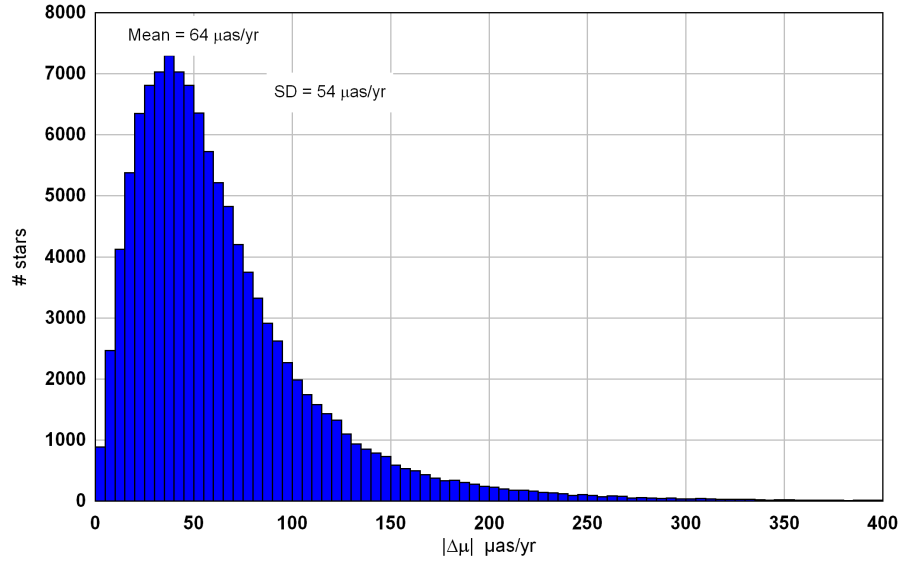


FIGURE 17: **Error on the annual sky motion**. Histogram of the errors in the annual displacement on the sky, measured by the increase of the distance between the true and computed position after one year.

The true error distribution is very useful to qualify the procedure, but not usable in the real case when the true values are unknown. It is replaced by some estimate of the uncertainty based on error propagation, including both random errors in the raw data and approximations or truncations in the modelling. To validate this estimate it is necessary to compare the true error to the estimated uncertainty.

The formal errors have been estimated from the first order modelling,

$$\mu_\alpha\, t = (\alpha_G - \alpha_H)\, \cos\delta_H \tag{24a}$$

$$\mu_\delta\, t = \delta_G - \delta_H \tag{24b}$$

with reference to the (H) Hipparcos and (G) Gaia positions. The standard error for the Gaia position is obtained from the least-squares fit of the observations to the 2-parameter model, using Hipparcos parallaxes and proper motion to refer the solution to the barycentric position and

by scaling the unit-weight-variance to the post-fit residuals. The corresponding standard deviations for Hipparcos are directly taken from the Catalogue. In practice the contribution resulting from the Hipparcos uncertainty at the first epoch is the largest of the two by a factor 3 or 4, meaning that the precise estimation of the modelling errors (assuming some nice averaging) in the processing of the Gaia observations is not crucial. Finally one has,

$$\sigma_{\mu_\alpha} = \sqrt{\sigma^2_{\alpha_G} + \sigma^2_{\alpha_H}}/t \tag{25a}$$

$$\sigma_{\mu_\delta} = \sqrt{\sigma^2_{\delta_G} + \sigma^2_{\delta_H}}/t \tag{25b}$$

The histograms of the reduced errors, that is to say the true errors measured in units of the estimated standard deviations given in (25), are plotted in Fig. 18-19. It is a good surprise to see that the distributions are nearly gaussian with zero mean and almost unit variance. This indicates that one will be able to estimate the statistical uncertainty with a simple error propagation model, despite the non random nature of most of the noise. This is true as long as the first epoch uncertainty remains the largest contributor, meaning that the correct evaluation of the standard deviation of the Gaia barycentric position is critical to obtain a fairly good estimate of the uncertainty of the proper motions. I also found that the standard deviations of the reduced distributions remain constant when the data is grouped in bins of magnitude.

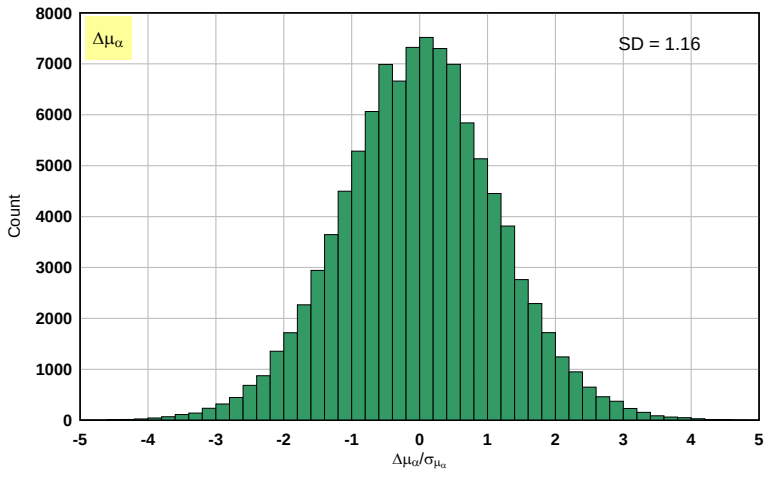


FIGURE 18: **Reduced errors for PM in right ascension**. Distribution of the reduced errors (error/$\sigma$) for the proper motion in right ascension. The standard deviation is 1.16 and the mean is not significantly different from zero.

### 6.2.2 Outliers

The next series of plots focusses on the tails of the error distributions. The plots are drawn as a function of the star ID number, roughly proportional to the right ascension, and are meant to show the outliers above or below the central part of the distribution. Figs. 20 - 21 display the true errors in $\mu$as/yr for right ascension and declination, while the next two figures, Fig. 22

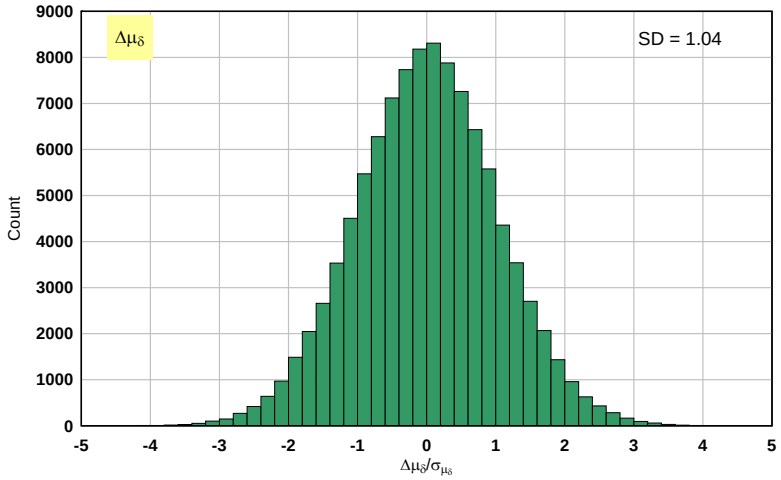


FIGURE 19: **Reduced errors for PM in declination**. Distribution of the reduced errors (error/$\sigma$) for the proper motion in declination. The standard deviation is 1.04 and the mean is not significantly different from zero.

- 23, provide a similar representation for the reduced errors. There are no real outliers, those that would be completely out of the distribution, and the largest errors are accounted for by the parallax uncertainty in the Hipparcos catalogue as shown later in the analysis of Fig. 25. The absence of outliers is more apparent in the reduced plots which smooth out the heterogeneity of the standard deviations. The corresponding diagrams are much more compact, with nothing abnormal outside the $3\sigma$ level. One sees also in Fig. 22 a small effect with right ascension (smaller scatter around $\alpha = 180$deg) hard to explain.

The last figure of this group (Fig. 24) gives for the declination the error distribution when the processing is done by using the first order formula to derive the proper motion (the plot for RA is very similar). This is the same idea as in Fig. 11, but now with a shifted reference catalogue contributing for most of the noise in the second epoch. Most of the outliers seen in Fig. 11 are still there but hidden in the statistical noise, and just the largest outliers (the very nearest stars) emerge on top of it. The difference between Fig. 21 and Fig. 24 is just the order in the inversion model, complete inversion vs. first order.

The errors in the computation of the proper motions come from the errors in position at the first and second epochs. For the first epoch, this is given by the Hipparcos accuracy ranging from 0.5 to 4 mas (data have been filtered out above 4 mas). At the second epoch, the main source of error is the approximate Hipparcos parallax used to find the barycentric position from the early Gaia apparent directions. The standard deviation of the Hipparcos parallax is about 1.3 that of the position (here taken as the mean between right ascension and declination). Therefore the error in the barycentric position at the second epoch, will increase exactly in the same way at that of the first epoch and if we take, for example, 4 mas for the combined error, this translates into about 200 $\mu$as/yr in the proper motion uncertainty, and for the tail of the distribution at $3\sigma$,

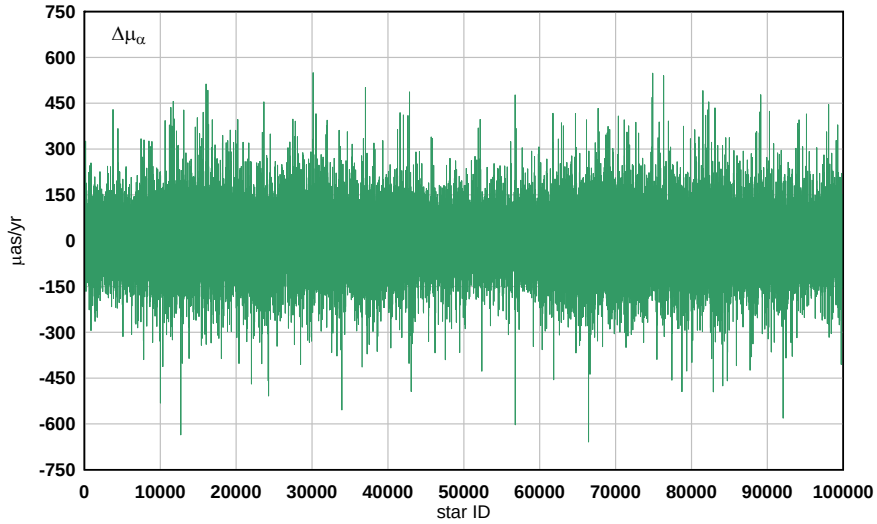


FIGURE 20: **Outliers for PM right ascension**. Distribution of the errors (computed - true value) for the proper motion in right ascension as a function of the star ID number. The central part of the diagram is saturated and the plot shows primarily the tails of the distribution.

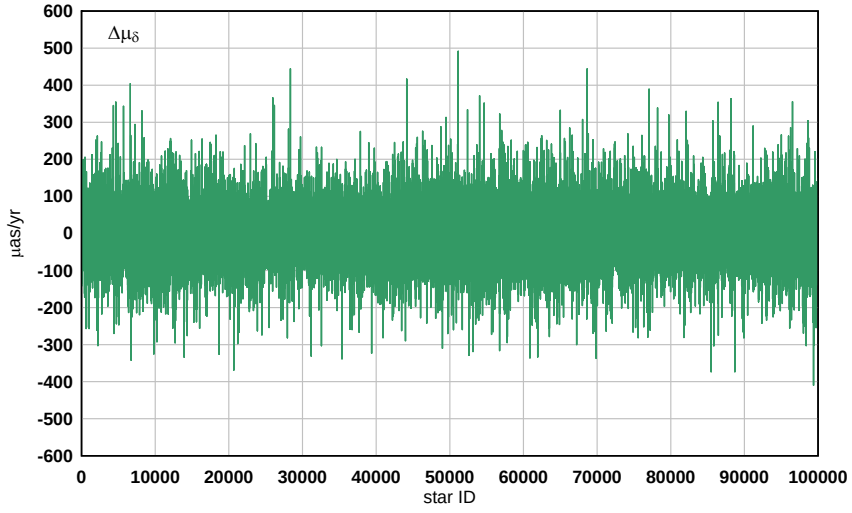


FIGURE 21: **Outliers for PM in declination**. Distribution of the errors (computed - true value) for the proper motion in declination as a function of the star ID number. The central part of the diagram is saturated and and the plot shows primarily the tails of the distribution.

something like 600 $\mu$as/yr. This effect is outstanding in Fig 25 where the absolute values of the true errors are plotted as a function of the Hipparcos astrometric accuracy. This feature accounts for the extended tails in the error distribution, not visible in the histograms, because the number of stars is too small. The estimated errors reproduce this effect and in the exploitation of the real data one would have the choice to filter out these stars, or to publish the result with the

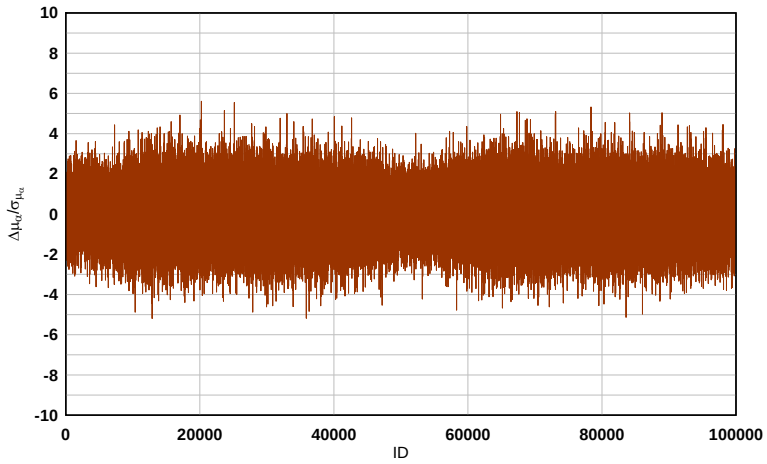


FIGURE 22: **Outliers for PM in right ascension with normalised errors**. Distribution of the reduced errors (error/$\sigma$) for the proper motion in right ascension as a function of the star ID number. The central part of the diagram is saturated and the plot shows primarily the tails and the outliers of the distribution.

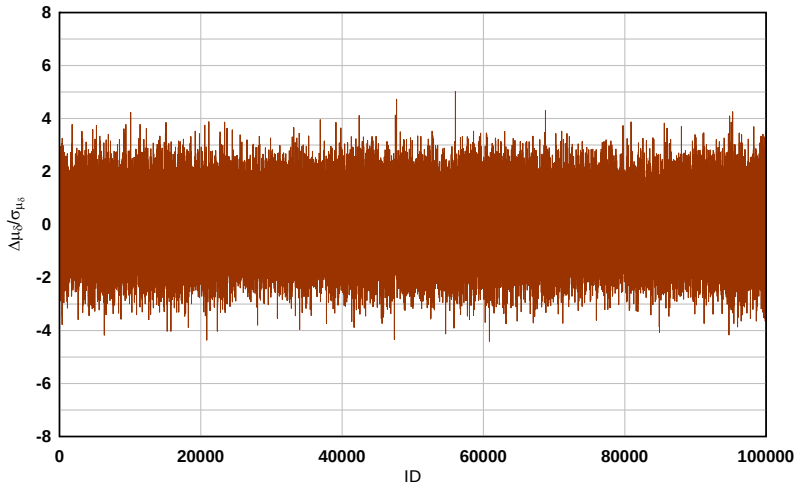


FIGURE 23: **Outliers for PM in declination with normalised errors**. Distribution of the reduced errors (error/$\sigma$) for the proper motion in declination as a function of the star ID number. The central part of the diagram is saturated and the plot shows primarily the tails and the outliers of the distribution.

corresponding large standard errors.

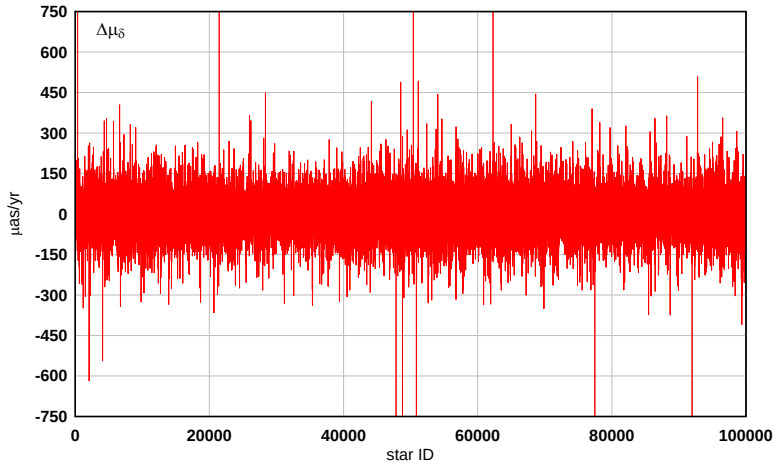


FIGURE 24: Distribution of the errors ((computed - true value)) for the proper motion in declination as a function of the star ID number. The central part of the diagram is saturated and and the plot shows primarily the tails of the distribution.

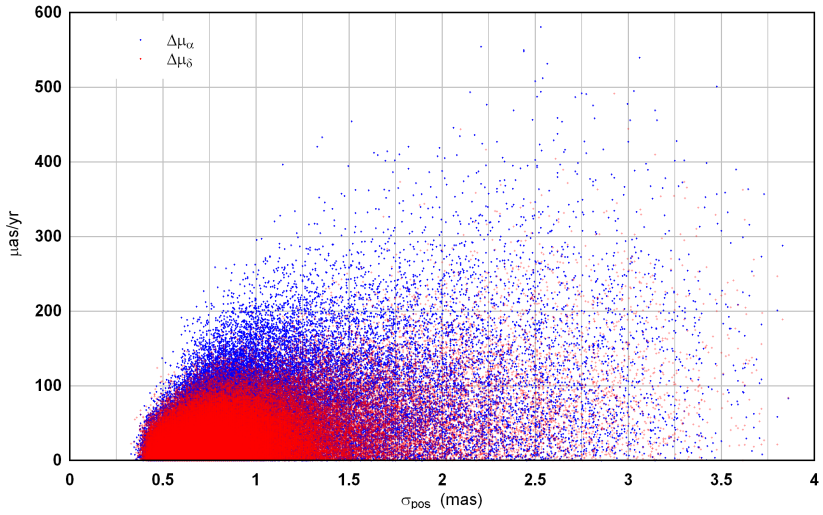


FIGURE 25: **Errors in PM vs. Hipparcos accuracy**. Scatter diagram showing the distribution of the absolute values of the true errors in proper motion (blue for RA and red for declination) as a function of the Hipparcos astrometric accuracy. The diagram shows the sensitivity of the accuracy of the proper motion to the quality of the reference catalogue used to process the Gaia observations.

Finally I have generated plots for the space distribution of the true errors and that of the estimated standard deviations computed with (25). The true errors are shown in Figs. 26-27, while the error in the annual displacement given by (23) is plotted in Fig. 28. The estimated errors are shown in Figs. 29-30 respectively in right ascension and declination. Not surprisingly, the signature of the scanning law (both from Hipparcos and Gaia) is significant in right ascension and almost not visible in declination. Due to the limited time coverage in Gaia, there is also a secondary irregularity as a function of the ecliptic longitude, resulting from the lack of uniformity of the number of observations.

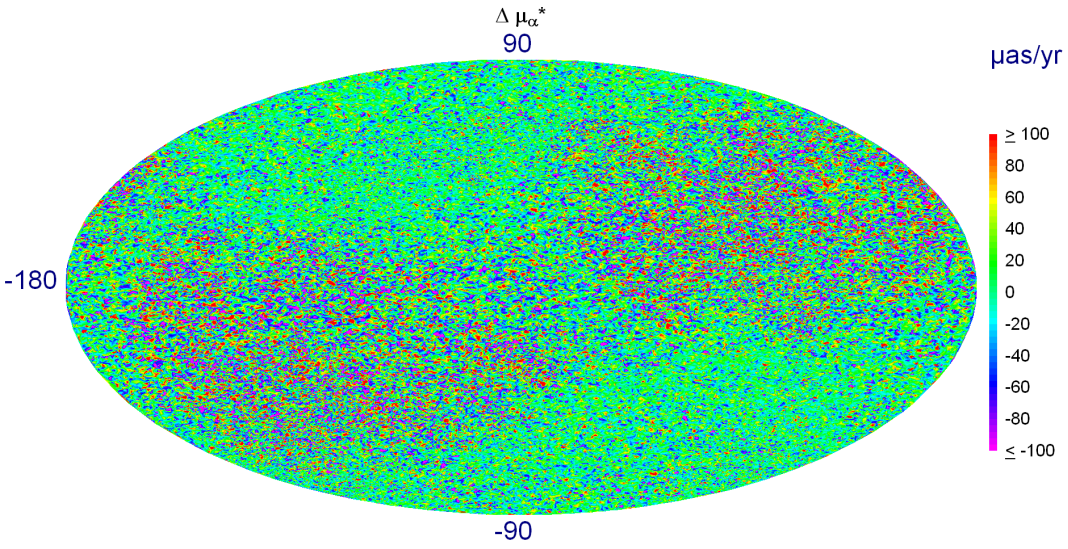


FIGURE 26: Spatial distribution of the true errors (computed - true value) for the proper motion component in right ascension. The lower precision around the ecliptic is inherited from the Hipparcos right ascension.

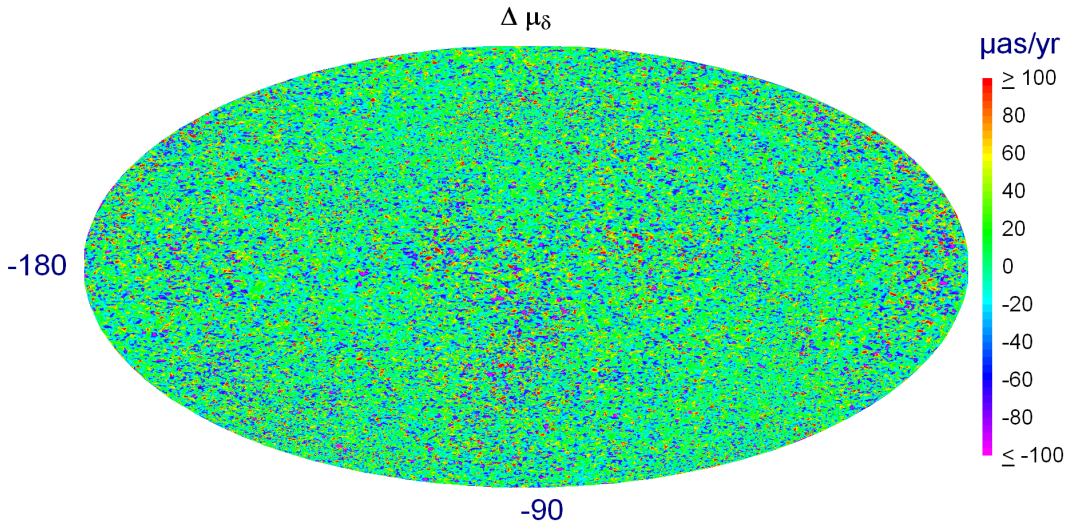


FIGURE 27: Spatial distribution of the true errors (computed - true value) for the proper motion component in declination.

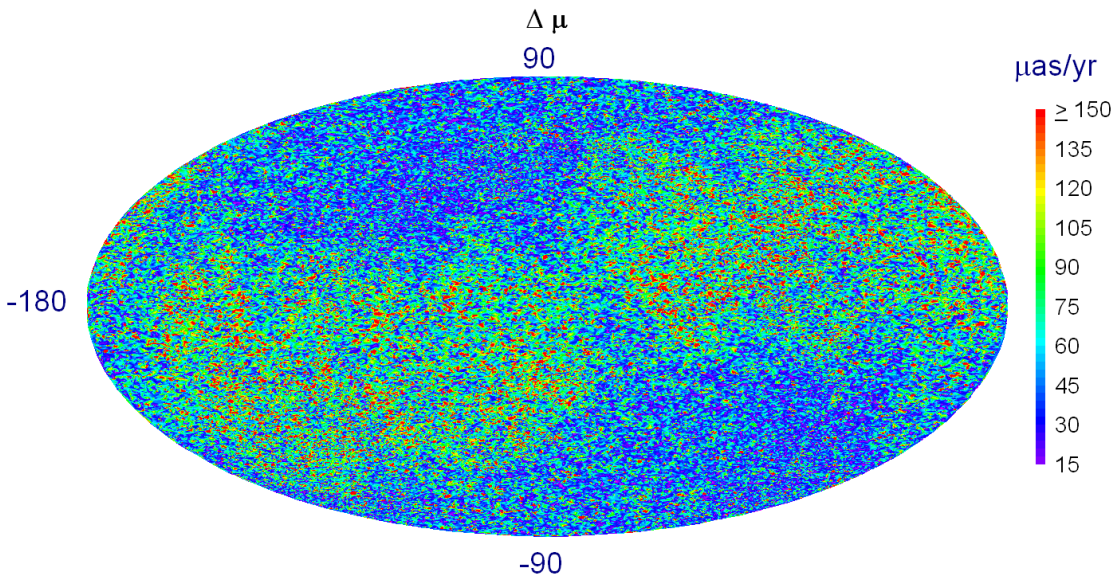


FIGURE 28: Spatial distribution of the error in annual displacement on the sky.

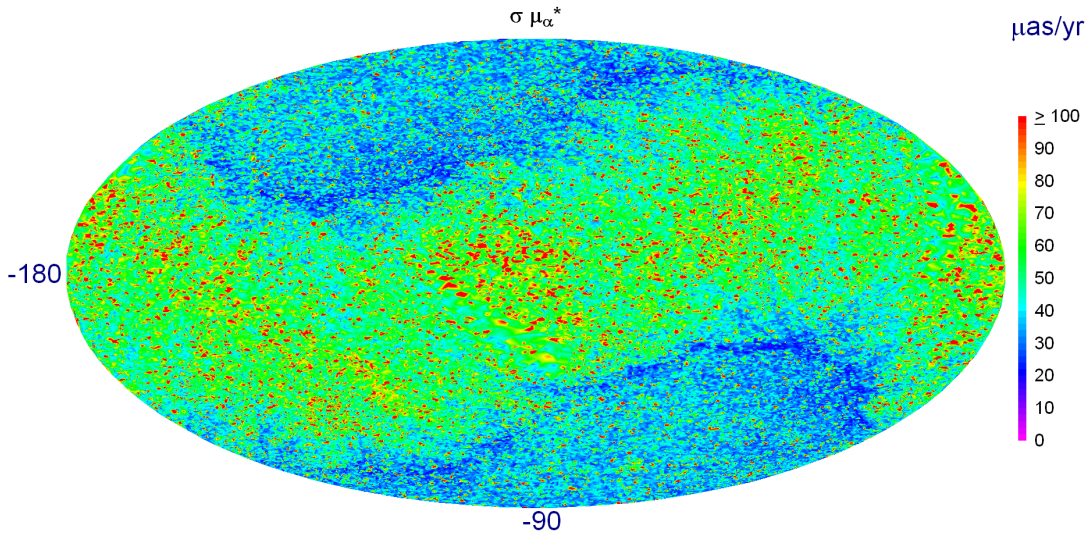


FIGURE 29: Spatial distribution of the estimated errors for the proper motion component in right ascension, with the expected ecliptic pattern inherited from Hipparcos.

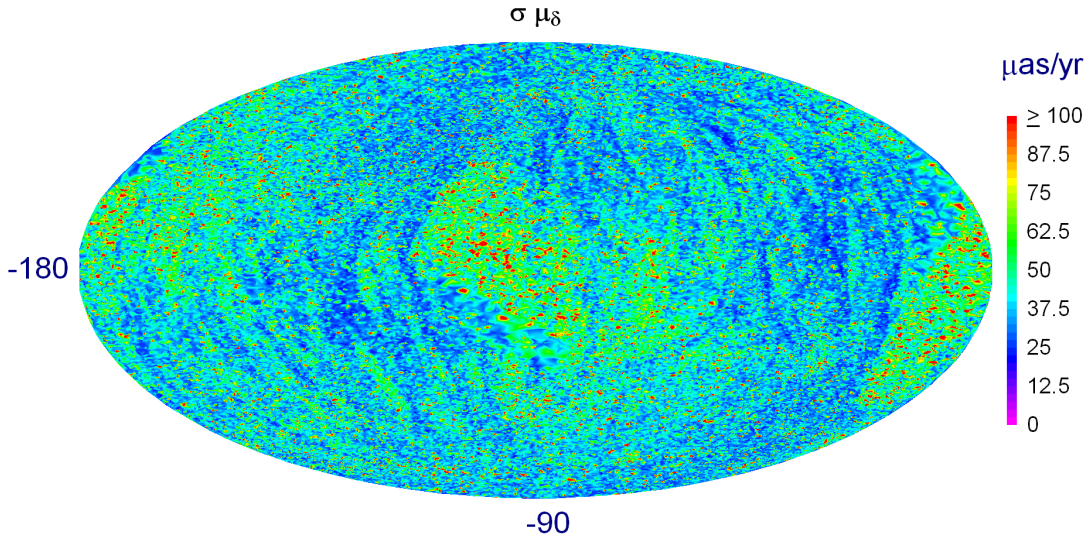


FIGURE 30: Spatial distribution of the estimated errors for the proper motion component in declination.

# 7 Additional issues

There are few more issues not discussed in this note which must be considered, primarily with the DPAC. They are listed below for further discussion.

- **The reference frame** Positions at two epochs can be combined to determine a proper motion, provided they are given in the same reference frame. Hipparcos has been brought into the ICRF, both in rotation and orientation at the end of the mission. The Hipparcos system is believed to be aligned with the extragalactic radio frame to within $0.6$ mas at the epoch 1991.25, and non-rotating with respect to distant extragalactic objects to within $0.25$ mas/yr (Kovalevsky et al. (1997)). Therefore, the early Gaia positions necessary to carry out the HTPM project must be in the same frame. Actually only the alignment matters, since one uses only positions and not proper motions. Given the number of sources in the recently released ICRF-2, each with a submas accuracy, this should not be a problem to align the Gaia solution to the ICRF with an accuracy of few 0.1 mas with a 6-month solution.

- **Light Propagation** The modelling presented in the first part has considered implicitly that the light propagates instantaneously. There is no distinction between the velocity measured by comparing positions at the reception time and the true velocity determined between two emission times. Since between the two epochs, the star distance has changed (when $v_r \neq 0$), there is a small effect in $v_r/c$ that enters the definition of the proper motion (Mignard (2003)). The correction is of the order of $10^{-4}$, and could be as large as 100$\mu$as/yr for the fast moving stars, then very relevant for this project. But this is more a question of definition of proper motion (something to propagate catalogue positions or true velocity to investigate the distribution of matter and the galactic potential) and must be decided on a more general basis for the whole Gaia catalogue.

- **AGIS solution for positions** A solution in AGIS with only two astrometric parameters per star is foreseen. But this can be done in several ways ending up either with a direction being the centre of the cluster of apparent directions seen by Gaia, or with the best estimate of the barycentric position at the middle of the interval covered by the observations. This depends how the conditions equations are written with the best available parallaxes and proper motions. By linearising the model in the neighbourhood of the best known values, and then keeping only the partial derivatives with respect to the barycentric coordinates will be sufficient.

- **Radial velocities availability** For all the nearby stars, say not farther than 30 pc, one needs relatively good radial velocities to deduce the proper motion at the first epoch from two independent positions. This is less mandatory for the other stars, but desirable to avoid small systematic effects that could show up in statistical studies.

Therefore one must look at the existing databases to see the availability and then to add the information into the Gaia auxiliary data.

- **Equations weighting** The Gaia measurements include the very accurate along-scan coordinate and the less accurate transverse coordinate. When a full astrometric model is used, the observation equations are weighed in proportion of the inverse of the variance of either measurements. But when the astrometric models is simplified, there are modelling errors much larger than the photon noise. If this modelling errors are somewhat random across the observation equations, they mimic a random noise that must be used for a proper scaling of the weighting. This has been done here from trials and errors and remains very crude and lacks a clear statistical justification. This again must be discussed with data processing experts to optimise the solution.

- **Which Hipparcos Catalogue?** I have used consistently the standard Hipparcos Catalogue for the accuracy assessment of the HTPM project. The new reduction of the Hipparcos data (van Leeuwen. (2005)), with better positions and better parallaxes should also lead to a better determination of the proper motions. This remains to be checked.

# 8 References

**[JDB-053]**, de Bruijne, J., 2009, *ALong- and ACross-scan location-estimation performance*, GAIA-CA-TN-ESA-JDB-053, URL http://www.rssd.esa.int/llink/livelink/open/2913726

Gontcharov G.A., 2006, Pulkovo Compilation of Radial Velocities for 35493 Hipparcos Stars in a Common System., Astronomy Letters, 32, 759-771.

Kovalevsky, J., Lindegren,L., M.A.C. Perryman, M.A.C et al., 1997, The Hipparcos Catalogue as a realisation of the extragalactic reference system, Astron. Astrophys. 323, 620-633.

Dravins, D., Lindegren, L., Madsen, S., 1999, Astrometric radial velocities. I. Non-spectroscopic methods for measuring stellar radial velocity, Astron. Astrophys., 348, 1040-1051.

Mignard, F., 2003, Considerations about the astrometric accuracy of Gaia, in Gaia Spectroscopy, Science and Technology, ASP Conf. Ser., U. Munari ed., 298, 25-40.

van de Kamp, P., 1967, Principles of Astrometry, W.H. Freeman.

van Leeuwen, F., Fantino, E., 2005, A new reduction of the raw Hipparcos data, Astron. Astrophys., 439, 791-803.

# A Central Projection

The projection and relevant notations are shown in Fig. 31, where $m$ is on the sphere and is projected on $M$ on the tangent plane to the sphere at $O$.

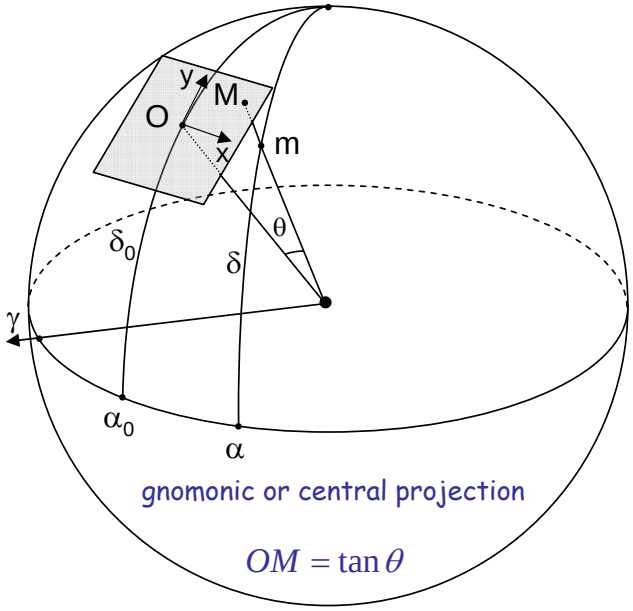


FIGURE 31: The general oblique central (or gnomonic) projection. The centre of projection is $O$ with coordinates $\alpha_0, \delta_0$, while $m$ is on the sphere with coordinates $\alpha, \delta$ and is centrally projected on the tangent plane at $O$ on $M$ with cartesian coordinates $x, y$.

If $\rho$ is the length $OM$ in the tangent plane, one has,

$$\rho = \tan\theta \tag{26}$$

Then if $\alpha_0, \delta_0$ (resp. $\alpha, \delta$) are the spherical coordinates of $O$ (resp. $m$), the cartesian coordinates of $M$ in the projection plane are given with basic spherical trigonometry by,

$$x = \frac{\cos\delta \sin(\alpha - \alpha_0)}{\sin\delta_0 \sin\delta + \cos\delta_0 \cos\delta \cos(\alpha - \alpha_0)} \tag{27a}$$

$$y = \frac{\cos\delta_0 \sin\delta - \sin\delta_0 \cos\delta \cos(\alpha - \alpha_0)}{\sin\delta_0 \sin\delta + \cos\delta_0 \cos\delta \cos(\alpha - \alpha_0)} \tag{27b}$$

Assuming that

$$a = \Delta\,\alpha\,\cos\delta_0 \tag{28a}$$
$$d = \Delta\,\delta \tag{28b}$$

are small quantities, the cartesian coordinates $x, y$ can be expanded in power of $a, d$. There are many ways, found in standard astronomical textbooks, to reduce the formulas to facilitate these expansions, but here I actually relied on computer algebra to find the expansions to the third order to find,

$$x = a - \tan\delta_0\, a\, d + \frac{3\cos^2\delta_0 - 1}{6\cos^2\delta_0}\, a^3 + \mathcal{O}(a^4, d^4) \tag{29a}$$
$$y = d + \frac{1}{2}\tan\delta_0\, a^2 + \frac{2\cos^2\delta_0 - 1}{2\cos^2\delta_0}\, a^2\, d + \frac{1}{3}d^3 + \mathcal{O}(a^4, d^4) \tag{29b}$$

and conversely,

$$\Delta\,\alpha\,\cos\delta_0 = x + \tan\delta_0\, x\, y + \tan^2\delta_0\, x\, y^2 - \frac{1}{3\,\cos^2\delta_0}\, x^3 + \mathcal{O}(x^4, y^4) \tag{30a}$$
$$\Delta\,\delta = y - \frac{1}{2}\,\tan\delta_0\, x^2 - \frac{1}{2\,\cos^2\delta_0}\, x^2\, y - \frac{y^3}{3} + \mathcal{O}(x^4, y^4) \tag{30b}$$

This has allowed to spot a mistake in a similar expression given in the astrometry book of van de Kamp (van de Kamp. (1967)), where the $xy^2$ term has a wrong $\sec^2\delta$ instead of $\sec\delta$.

It is sometimes interesting to express the projection with $\delta$ instead of $\delta_0$ in the plate projection equations (gnomonic projection). The corresponding formulas are as follows,

$$\bar{a} = \Delta\,\alpha\,\cos\delta \tag{31a}$$
$$d = \Delta\,\delta \tag{31b}$$

leading for the direction transformation,

$$x = \bar{a} + \frac{3\cos^2\delta - 1}{6\cos^2\delta}\,\bar{a}^3 + \frac{1}{2}\,\bar{a}\,d^2 + \mathcal{O}(\bar{a}^4, d^4) \tag{32a}$$
$$y = d + \frac{1}{2}\tan\delta\,\bar{a}^2 + \frac{1}{3}d^3 + \mathcal{O}(\bar{a}^4, d^4) \tag{32b}$$

and conversely,

$$\Delta\,\alpha\,\cos\delta = x - \frac{1}{2}\,x\,y^2 - \frac{3\cos^2\delta - 1}{6\,\cos^2\delta}\,x^3 + \mathcal{O}(x^4, y^4) \tag{33a}$$
$$\Delta\,\delta = y - \frac{1}{2}\,\tan\delta\,x^2 - \frac{y^3}{3} + \mathcal{O}(x^4, y^4) \tag{33b}$$

with this time a sign error in van de Kamp for the $x^3$ term. One must notice the absence of second order term in $x(\bar{a}, d)$ and $\Delta\,\alpha\,\cos\delta(x, y)$, meaning that the equation $\Delta\,\alpha\,\cos\delta = x$ (with $\delta$ and not $\delta_0$) is correct to second order, but this fortunate circumstance does not apply to the pair $(y, \Delta\,\delta)$.

# B Parallel projection

The projection and relevant notations are shown in Fig. 32, where $m$ is on the sphere and is projected on $M$ on the tangent plane to the sphere at $O$.

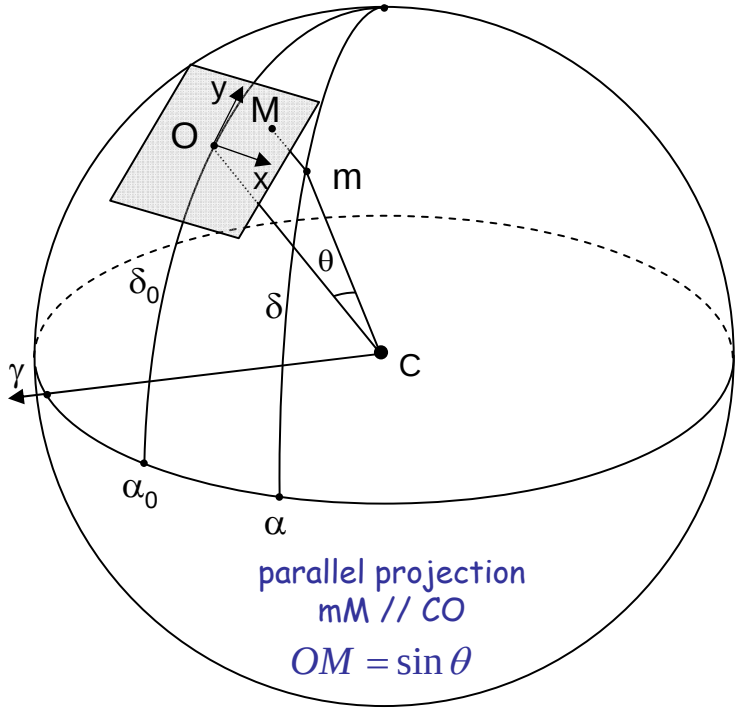


FIGURE 32: The general oblique parallel (or orthographic) projection. The centre of projection is $O$ with coordinates $\alpha_0, \delta_0$ while $m$ lies on the sphere with coordinates $\alpha, \delta$ and is parallel projected on the tangent plane on $M$ with cartesian coordinates $x, y$.

If $\rho$ is the length $OM$ in the tangent plane, one has,

$$\rho = \sin\theta \tag{34}$$

Then if $\alpha_0, \delta_0$ (resp. $\alpha, \delta$) are the spherical coordinates of $O$ (resp. $m$), the cartesian coordinates of $M$ in the projection plane are given from simple spherical trigonometry by,

$$x = \cos\delta \sin(\alpha - \alpha_0) \tag{35a}$$
$$y = \cos\delta_0 \sin\delta - \sin\delta_0 cos\delta \cos(\alpha - \alpha_0) \tag{35b}$$

Then, as for the central projection, one introduces the notations,

$$a = \Delta\,\alpha\,\cos\delta_0 \tag{36a}$$
$$d = \Delta\,\delta \tag{36b}$$

to write the expansions of $x, y$ in power of $a, d$ to the third order as,

$$x = a - \tan\delta_0\, a\, d - \frac{a^3}{6\cos^2\delta_0} - \frac{1}{2}\, a\, d^2 + \mathcal{O}(a^4, d^4) \tag{37a}$$
$$y = d + \frac{1}{2}\tan\delta_0\, a^2 - \frac{1}{2}\,\tan^2\delta_0\, a^2\, d - \frac{1}{6}d^3 + \mathcal{O}(a^4, d^4) \tag{37b}$$

Here one can see the difference with the central projection in the third order terms, both in $x$ and $y$. Conversely, again with Maple to solve for $a, d$ by analytical fixed point iterations,

$$\Delta\,\alpha\,\cos\delta_0 = x + \tan\delta_0\, x\, y + \left(\frac{1}{2} + \tan^2\delta_0\right) x\, y^2 + \frac{1 - 3\sin^2\delta_0}{6\,\cos^2\delta_0}\, x^3 + \mathcal{O}(x^4, y^4) \tag{38a}$$
$$\Delta\,\delta = y - \frac{1}{2}\,\tan\delta_0\, x^2 - \frac{1}{2}\,\tan^2\delta_0\, x^2\, y + \frac{y^3}{6} + \mathcal{O}(x^4, y^4) \tag{38b}$$

# C Alternate derivation of the propagation model

Consider again the basic kinematical model with a uniform rectilinear motion in the Euclidean space. It is characterized by the fact that the velocity vector is parallel transported along the geodesic of the underlying space, i.e along a straight line. There are different ways to obtain the corresponding components of the coordinate acceleration, however the most direct consists of expressing that the 3-D acceleration $d^2\mathbf{r}/dt^2 = 0$ and finding the components of the acceleration in spherical coordinates. In curvilinear coordinates $y^i$ one has for the covariant derivative,

$$\gamma^i = \frac{d^2y^i}{dt^2} + \Gamma^i_{jk}\,\frac{dy^j}{dt}\,\frac{dy^k}{dt} \tag{39}$$

where the Christoffel symbols $\Gamma^i_{jk}$ are computed from the metric of $R_3$ in spherical coordinates,

$$ds^2 = dr^2 + r^2\,\cos^2\delta\,d\alpha^2 + r^2\,d\delta^2 \tag{40}$$

using $y^1 = r$, $y^2 = \alpha$, $y^3 = \delta$, which gives in the local frame (normalised with unit vectors) $\mathbf{e}_r, \mathbf{e}_\alpha, \mathbf{e}_\delta$ the non-zero Christoffel symbols,

$$\Gamma^1_{22} = -r\,\cos^2\delta \tag{41a}$$
$$\Gamma^1_{33} = -r \tag{41b}$$
$$\Gamma^2_{12} = 1/r \tag{41c}$$
$$\Gamma^2_{23} = -\tan\delta \tag{41d}$$
$$\Gamma^3_{13} = 1/r \tag{41e}$$
$$\Gamma^3_{22} = \sin\delta\,\cos\delta \tag{41f}$$

Then with $\gamma^i = 0$ for a uniform rectilinear motion one has,

$$\ddot{r} = r\cos^2\delta\;\dot{\alpha}^2 + r\,\dot{\delta}^2 \tag{42a}$$
$$\ddot{\alpha} = -\frac{2}{r}\,\dot{r}\,\dot{\alpha} + 2\tan\delta\,\dot{\alpha}\dot{\delta} \tag{42b}$$
$$\ddot{\delta} = -\frac{2}{r}\,\dot{r}\dot{\delta} - \sin\delta\cos\delta\,\dot{\alpha}^2 \tag{42c}$$

Eqs. 42b-42c are the general expressions for the second derivatives of the right ascension and declination of a star moving on a straight line at constant speed in space. There are supplementary terms of the same order of magnitude which are different from zero even in the case of a purely tangential motion.

Now one can write the propagation model as,

$$\alpha(t) = \alpha_0 + \dot{\alpha}\, t + \ddot{\alpha}\, \frac{t^2}{2} \tag{43a}$$

$$\delta(t) = \delta_0 + \dot{\delta}\, t + \ddot{\delta}\, \frac{t^2}{2} \tag{43b}$$

or with Equations (42) and $\mu_\alpha = \dot{\alpha}\, \cos\delta_0$, $\mu_\delta = \dot{\delta}$

$$\Delta\alpha \cos\delta_0 = \mu_\alpha\, t - \left[\mu_r\, \mu_\alpha - \tan\delta_0\, \mu_\alpha\, \mu_\delta\right]\, t^2 \tag{44a}$$

$$\Delta\delta = \mu_\delta\, t - \left[\mu_r\, \mu_\delta + \frac{\tan\delta_0}{2}\, \mu_\alpha^2\right]\, t^2 \tag{44b}$$

which can be inverted to second order to get $\mu_\alpha$ and $\mu_\delta$ as a function of the displacement between the two epochs. This yields, by using as before

$$a = \Delta\,\alpha\, \cos\delta_0 \tag{45}$$

$$d = \Delta\,\delta \tag{46}$$

$$\mu_\alpha\, t = a(1 + \mu_r\, t) - \tan\delta_0\, a\, d \tag{47a}$$

$$\mu_\delta\, t = d\,(1 + \mu_r\, t) + \frac{1}{2}\tan\delta_0\, a^2 \tag{47b}$$

The same can be extended to third order without too much problem. By differentiating Eqs. 42 with respect to time and inserting back the component of the acceleration one obtains the third time derivative expressed as function of $\dot{r}$, $\dot{\alpha}$ and $\dot{\beta}$, or better as a function $\mu_r, \mu_\alpha, \mu_\delta$. One gets,

$$\frac{d^3\alpha}{dt^3} = 6\,\frac{\dot{r}^2}{r^2}\,\dot{\alpha} - 12\tan\delta\,\frac{\dot{r}}{r}\dot{\alpha}\dot{\delta} + 6\tan^2\delta\,\dot{\alpha}\dot{\delta}^2 - 2\dot{\alpha}^3 \tag{48a}$$

$$\frac{d^3\delta}{dt^3} = 6\,\frac{\dot{r}^2}{r^2}\,\dot{\delta} + 3\,\sin 2\delta\,\frac{\dot{r}}{r}\dot{\alpha}^2 - 3\,\dot{\alpha}^2\,\dot{\delta} - 2\dot{\delta}^3 \tag{48b}$$

and now with

$$\alpha(t) = \alpha_0 + \dot{\alpha}\, t + \ddot{\alpha}\, \frac{t^2}{2} + \dddot{\alpha}\, \frac{t^3}{6} \tag{49a}$$

$$\delta(t) = \delta_0 + \dot{\delta}\, t + \ddot{\delta}\, \frac{t^2}{2} + \dddot{\delta}\, \frac{t^3}{6} \tag{49b}$$

and with the introduction of the $\mu_r, \mu_\alpha, \mu_\delta$ one gets,

$$\begin{aligned}\Delta\alpha\cos\delta_0 = \mu_\alpha\, t - [\mu_r\,\mu_\alpha - \tan\delta_0\,\mu_\alpha\,\mu_\delta]\; t^2 \\ + \left[\mu_r^2\,\mu_\alpha - 2\tan\delta_0\,\mu_r\,\mu_\alpha\,\mu_\delta + \tan^2\delta\,\mu_\alpha\,\mu_\delta^2 - \frac{\mu_\alpha^3}{3\,\cos^2\delta_0}\right] t^3\end{aligned} \tag{50}$$

$$\begin{aligned}\Delta\delta = \mu_\delta\, t - \left[\mu_r\,\mu_\delta + \frac{\tan\delta_0}{2}\,\mu_\alpha^2\right] t^2 \\ + \left[\mu_r^2\,\mu_\delta + \tan\delta_0\,\mu_r\,\mu_\alpha^2 - \frac{\mu_\alpha^2\,\mu_\delta}{2\,\cos^2\delta_0} - \frac{\mu_\delta^3}{3}\right] t^3\end{aligned} \tag{51}$$

Equations (50)-(51) give the propagation model to third order of the proper motions and are similar in content to equations (17)-(18). Solving now this system for $\mu_\alpha$ and $\mu_\delta$, or equivalently inverting the series to the same order is much more involved than for the second degree. It can be achieved with a fixed point iteration repeated twice, starting with $\mu_\alpha\, t = \Delta\alpha\cos\delta_0 \equiv a$ and $\mu_\delta\, t = \Delta\delta \equiv d$. This is tedious with pencil and paper and I actually let Maple do it for me quickly and reliably. The process leads to the final transformation,

$$\mu_\alpha\, t = a(1+\mu_r\, t) - \tan\delta_0\, a\, d + \frac{3\cos^2\delta_0 - 1}{6\,\cos^2\delta_0}\, a^3 - \tan\delta_0\, a\, d\,\mu_r t \tag{52a}$$

$$\mu_\delta\, t = d\,(1+\mu_r\, t) + \frac{1}{2}\tan\delta_0\, a^2 + \frac{2\cos^2\delta_0 - 1}{2\,\cos^2\delta_0}\, a^2\, d + \frac{1}{2}\tan\delta_0\, a^2\,\mu_r t + \frac{d^3}{3} \tag{52b}$$

which is exactly the same as equations (15)-(16).

**Remark:** Using indices algebra, Eqs. (48), could have been directly derived from a straight differentiation of Eq. (39) with $\gamma^i = 0$. This gives,

$$\frac{d^3 y^i}{dt^3} = \left[-\frac{\partial\Gamma^i_{jk}}{\partial y^l} + 2\Gamma^i_{mj}\,\Gamma^m_{kl}\right] \dot{y^j}\,\dot{y^k}\,\dot{y^l} \tag{53}$$

and with the substitution of (41) one gets the same as (48).